

UNWB1 - 1721

WM RECORD COPY

SANDIA REPORT

SAND84-0369 • Unlimited Release • UC-70

Printed July 1985

WM DOCKET CONTROL
CENTER

Nevada Nuclear Waste Storage Investigations Project '85 AUG 12 A11:52

Vadose Water Flow Around a Backfilled Drift Located in Tuff

Lisa A. Mondy, Bruce L. Baker, Roger R. Eaton

Prepared by
Sandia National Laboratories
Albuquerque, New Mexico 87185 and Livermore, California 94550
for the United States Department of Energy
under Contract DE-AC04-76DP00789

HYDROLOGY DOCUMENT NUMBER 138

Issued by Sandia National Laboratories, operated for the United States Department of Energy by Sandia Corporation.

NOTICE: This report was prepared as an account of work sponsored by an agency of the United States Government. Neither the United States Government nor any agency thereof, nor any of their employees, nor any of their contractors, subcontractors, or their employees, makes any warranty, express or implied, or assumes any legal liability or responsibility for the accuracy, completeness, or usefulness of any information, apparatus, product, or process disclosed, or represents that its use would not infringe privately owned rights. Reference herein to any specific commercial product, process, or service by trade name, trademark, manufacturer, or otherwise, does not necessarily constitute or imply its endorsement, recommendation, or favoring by the United States Government, any agency thereof or any of their contractors or subcontractors. The views and opinions expressed herein do not necessarily state or reflect those of the United States Government, any agency thereof or any of their contractors or subcontractors.

Printed in the United States of America
Available from
National Technical Information Service
U.S. Department of Commerce
5285 Port Royal Road
Springfield, VA 22161

NTIS price codes
Printed copy: A04
Microfiche copy: A01

SAND84-0369
Unlimited Release
Printed July 1985

Distribution
UC-70

VADOSE WATER FLOW AROUND A BACKFILLED DRIFT LOCATED IN TUFF

Lisa A. Mondy
Fluid Mechanics and Heat Transfer Division I
Sandia National Laboratories, Albuquerque, New Mexico 87185

Bruce L. Baker
Technadyne Engineering Consultants, Inc.
Albuquerque, New Mexico 87111

Roger R. Eaton
Fluid Mechanics and Heat Transfer Division I
Sandia National Laboratories, Albuquerque, New Mexico 87185

ABSTRACT

Through the technique of computer simulation, the authors investigate the flow characteristics of groundwater from surface influx into a host medium of unsaturated tuff. The study is designed to assess the potential influence of backfilled drifts on the groundwater flow past vertically emplaced waste canisters in a prospective nuclear waste repository. Numerical modeling with the code SAGUARO is used to determine the magnitude and direction of flow in the vicinity of a waste package below a drift backfilled with various materials. Sand and clay represent potential backfill materials which are significantly different in hydrologic properties. Results indicate that clay in a drift reduces the flow immediately adjacent to the waste package to 91 to 96% of the natural flow. Sand in the same drift acts as an extremely effective barrier to flow; however, below the drift at the waste package level, the groundwater flow is 81% to 92% of the natural volumetric flow. Therefore, backfilling a drift does not provide a significant reduction of flow in the vicinity of a vertically emplaced waste package. The effect of the drift on flow extends only slightly over a drift length below and a drift width to the side of the backfilled region.

CONTENTS

	<u>Page</u>
1. INTRODUCTION	8
2. A DESCRIPTION OF SAGUARO AND THE MODELS ANALYZED	11
3. MATERIAL PROPERTIES AND INITIAL CONDITIONS	14
4. NUMERICAL INSTABILITIES WHEN MODELING SAND	23
5. RESULTS	26
6. SUMMARY AND CONCLUSIONS	60
ACKNOWLEDGEMENTS	61
REFERENCES	62

FIGURES

	<u>Page</u>
1. Simplified cross-section of a drift in the floor emplacement configuration	9
2. Finite-element mesh with drift and waste package outlined in bold (not to scale -- horizontal axis has been stretched to show detail)	12
3. Permeability vs pressure head -- characteristic curves for tuff, clay, and sand	15
4. Saturation vs pressure head -- characteristic curves for tuff, clay, and sand (Note that the kink in the curve for clay is an artifact of the spline fit used and that it is not in the pressure range of interest).	16
5. Derivative of saturation with respect to pressure head -- characteristic curve for tuff	17
6. Derivative of saturation with respect to pressure head -- characteristic curve for clay	18
7. Derivative of saturation with respect to pressure head -- characteristic curve for sand	19
8. Modified permeability characteristic curve for sand	21
9. Contours of constant effective pressure at time = 50 years for a clay-filled drift	27
10. Contours of constant effective pressure at time = 109 years for a clay-filled drift	28
11. Contours of constant effective pressure at time = 600 years (steady state) for a clay-filled drift (not to scale -- horizontal axis has been stretched to show detail)	29
12. Contours of constant effective pressure at time = 600 years for an impermeable drift (not to scale -- horizontal axis has been stretched to show detail)	30
13. Close-up of the finite-element mesh in the vicinity of the drift and waste package	33

	<u>Page</u>
14. Velocity vectors of steady-state flow near a sand-filled drift (sand modeled with modified permeability and as an impermeable material)	40
15. Steady-state profile of the horizontal components of velocities along a path (shown with the dotted line on the element grid above) from below the waste package through a clay-filled drift to the top boundary	41
16. Steady-state profile of the vertical components of velocities along a path (shown with the dotted line on the element grid above) from below the waste package through a clay-filled drift to the top boundary	42
17. Steady-state profile of the horizontal components of velocities along a path (shown with the dotted line on the element grid above) approximately 2.3 m to the side of a clay-filled drift	43
18. Steady-state profile of the vertical components of velocities along a path (shown with the dotted line on the element grid above) approximately 2.3 m to the side of a clay-filled drift	44
19. Steady-state profile of the horizontal components of velocities along a path (shown with the dotted line on the element grid above) through a clay-filled drift from the left to the right side boundary	45
20. Steady-state profile of the vertical components of velocities along a path (shown with the dotted line on the element grid above) through a clay-filled drift from the left to the right side boundary	46
21. Steady-state profile of the horizontal components of velocities along a path (shown with the dotted line on the element grid above) from below the waste package through an impermeable drift to the top boundary	47
22. Steady-state profile of the vertical components of velocities along a path (shown with the dotted line on the element grid above) from below the waste package through an impermeable drift to the top boundary	48

23. Steady-state profile of the horizontal components of velocities along a path (shown with the dotted line on the element grid above) approximately 2.3 m to the side of an impermeable drift 49

24. Steady-state profile of the vertical components of velocities along a path (shown with the dotted line on the element grid above) approximately 2.3 m to the side of an impermeable drift 50

25. Steady-state profile of the horizontal components of velocities along a path (shown with the dotted line on the element grid above) through an impermeable drift from the left to the right side boundary 51

26. Steady-state profile of the vertical components of velocities along a path (shown with the dotted line on the element grid above) through an impermeable drift from the left to the right side boundary 52

27. Steady-state profile of the horizontal components of velocities along a path (shown with the dotted line on the element grid above) from below the waste package through a (modified permeability) sand-filled drift to the top boundary 54

28. Steady-state profile of the vertical components of velocities along a path (shown with the dotted line on the element grid above) from below the waste package through a (modified permeability) sand-filled drift to the top boundary 55

29. Steady-state profile of the horizontal components of velocities along a path (shown with the dotted line on the element grid above) approximately 2.3 m to the side of a (modified permeability) sand-filled drift 56

30. Steady-state profile of the vertical components of velocities along a path (shown with the dotted line on the element grid above) approximately 2.3 m to the side of a (modified permeability) sand-filled drift 57

31. Steady-state profile of the horizontal components of velocities along a path (shown with the dotted line on the element grid above) through a (modified permeability) sand-filled drift from the left to the right side boundary 58
32. Steady-state profile of the vertical components of velocities along a path (shown with the dotted line on the element grid above) through a (modified permeability) sand-filled drift from the left to the right side boundary 59

TABLES

	<u>Page</u>
1. MATERIAL PROPERTIES	14
2. INITIAL SATURATION CONDITIONS	22
3. STEADY-STATE CONDITIONS	
(Infiltration rate = 0.4 cm/yr)	31
4. STEADY-STATE FLOW THROUGH THE CLAY-FILLED DRIFT	32
5. STEADY-STATE FLOW INSIDE THE CLAY-FILLED DRIFT	34
6. VELOCITIES IN TUFF NEAR DRIFT AND WASTE PACKAGE WITH A CLAY-FILLED DRIFT	35
7. VELOCITIES IN TUFF NEAR DRIFT AND WASTE PACKAGE WITH A (MODIFIED) SAND-FILLED DRIFT	37
8. VELOCITIES IN TUFF NEAR DRIFT AND WASTE PACKAGE WITH AN IMPERMEABLE DRIFT	38

1. INTRODUCTION

The purpose of the Nevada Nuclear Waste Storage Investigations (NNWSI) Project, managed by the Nevada Operations Office of the U. S. Department of Energy, is to examine the feasibility of siting a repository for high-level nuclear waste at Yucca Mountain on, and adjacent to, the Nevada Test Site. As part of these investigations, Sandia National Laboratories is engaged in evaluating the need for backfilling and sealing of this prospective nuclear waste repository located in an unsaturated tuff environment. In this report, we describe a computer analysis of groundwater influx in the vicinity of repository drifts when the drifts are filled with either sand or clay and discuss how these two backfills affect the flow past the waste package.

Hydrologic characteristic curves for a sand, a clay, and a welded tuff were chosen for use in these analyses: the clay and sand to represent materials with quite different hydrologic behavior, and the tuff to represent a type of host rock possible in a provisional nuclear waste repository [7]. The sand contains mostly coarse-sized particles and is highly permeable when saturated. The clay contains many fine-sized particles and, so, is less permeable than sand when saturated. However, the permeability of unsaturated sand can be far smaller than that of clay. When unsaturated, both sand and clay can be less permeable than tuff.

A simplified geometry (shown in Figure 1) represents a cross-section of a drift and a waste canister in the floor emplacement configuration, in which the waste canisters are placed in vertical emplacement holes spaced along the drift centerline with isolation plugs sealing the individual emplacement holes. The water is assumed to be influx from the surface flowing past this drift. The finite-element code SAGUARO [1] is used to describe two-dimensional, isothermal, flow through the porous matrix in this geometry. Flow in fractures is not being considered.

Because the permeability of sand varies dramatically with saturation and this in turn causes numerical instabilities, we use two methods to simulate sand in the drift. The first method is to modify the assumed properties of the sand. The second is to model sand as an impermeable material. The hydrologic properties of clay cause no numerical problems, and, hence, are used without modification.

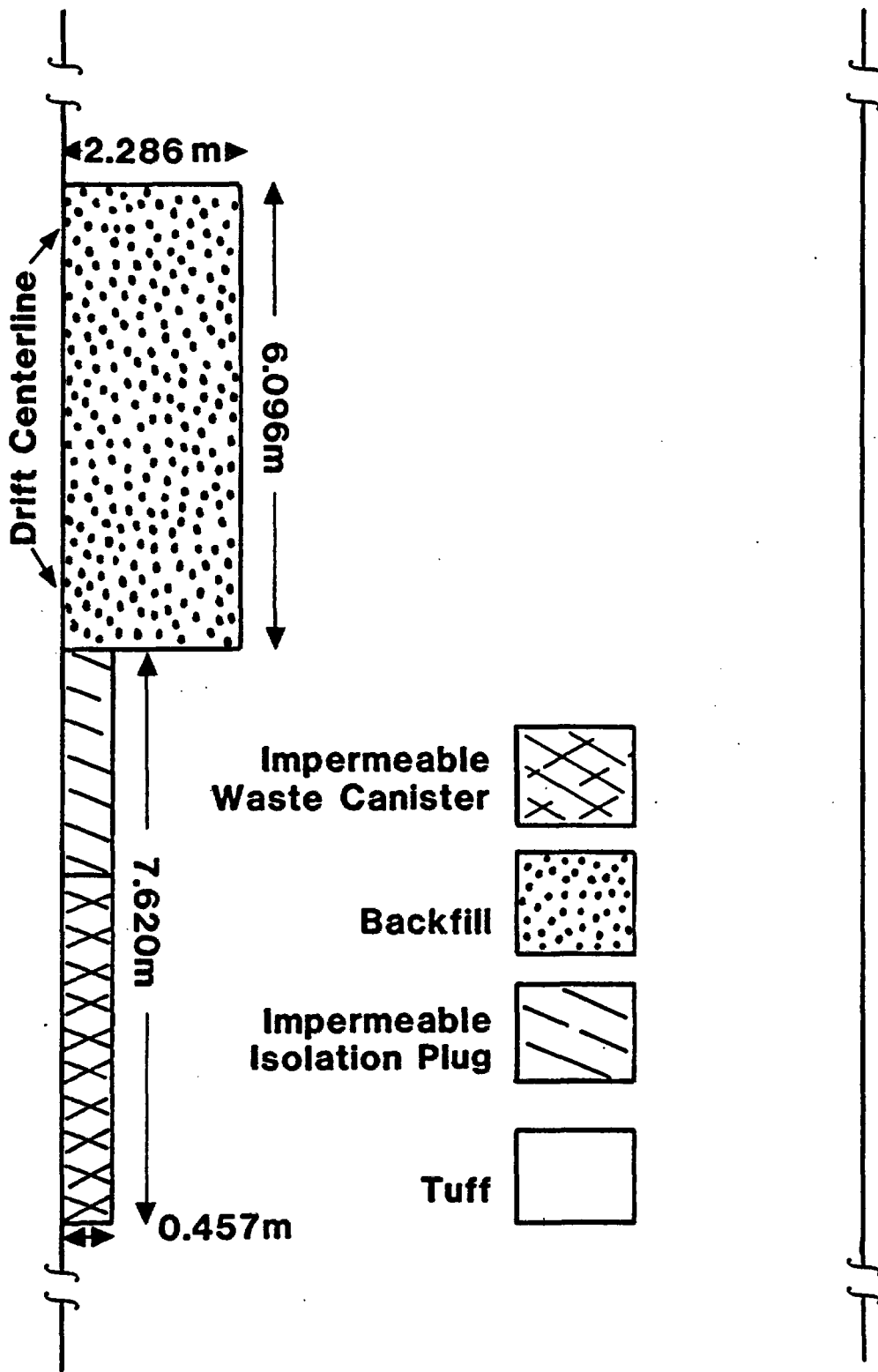


Figure 1. Simplified cross-section of a drift in the floor emplacement configuration.

This report contains:

- A description of the numerical model
- A discussion of the properties of the materials used in the analyses
- A discussion of the numerical instabilities encountered when modeling sand
- The expected steady-state velocities near the various backfilled drifts and waste packages
- The expected flow through the various backfilled drifts at steady state.

2. A DESCRIPTION OF SAGUARO AND THE MODELS ANALYZED

The authors use SAGUARO, a finite-element code developed by Eaton, et al. [1], to model the flow of vadose water near a vertically emplaced nuclear waste package. For isothermal flows, SAGUARO solves the well-known Richards equation [2], which has the form:

$$\frac{\partial}{\partial x_i} \left(\frac{k_{ij}}{\mu} \frac{\partial \phi}{\partial x_j} \right) = \frac{1}{\rho g} C \frac{\partial \phi}{\partial t} \quad (1)$$

Here k_{ij} is the intrinsic permeability tensor and μ is the dynamic viscosity of water. ϕ is the effective pressure, i.e. the hydrodynamic pressure plus the pressure due to gravity,

$$\phi = \rho g (\Psi + z) \quad , \quad (2)$$

where Ψ is the pressure head ($P/\rho g$); ρ is the density of water; and g is the acceleration due to gravity. The specific moisture capacity C , is the derivative of the moisture content with respect to pressure head ($\partial \theta / \partial \Psi$). For unsaturated flow, the properties k_{ij} and C are strongly dependent on Ψ . Thus, equation (1) is highly non-linear. Finally, Equation (1) describes the flow through the porous matrix. Although highly fractured regions of tuff may exist, this study does not address the issue of flow through fractures.

Figure 1 illustrates the two-dimensional approximation of the geometry of the drift and waste canister modeled. In this representation, we assume that the plug and waste package are impermeable. Note that in this two-dimensional representation, all zones are treated as semi-infinite slabs extending in the direction perpendicular to the plane of Figure 1. Figure 2 shows the finite-element mesh used.

As the rock is unsaturated, we assume that the source of groundwater movement is the influx of rainwater from the surface above. (We are assuming that liquid free convection due to the heat release by the waste is negligible in unsaturated porous media [3]. Vapor flow cannot be addressed with SAGUARO.) We assume a constant velocity of 0.4 cm/yr (1.097×10^{-5} m/day) at the upper boundary of our model [4] and impose a constant pressure

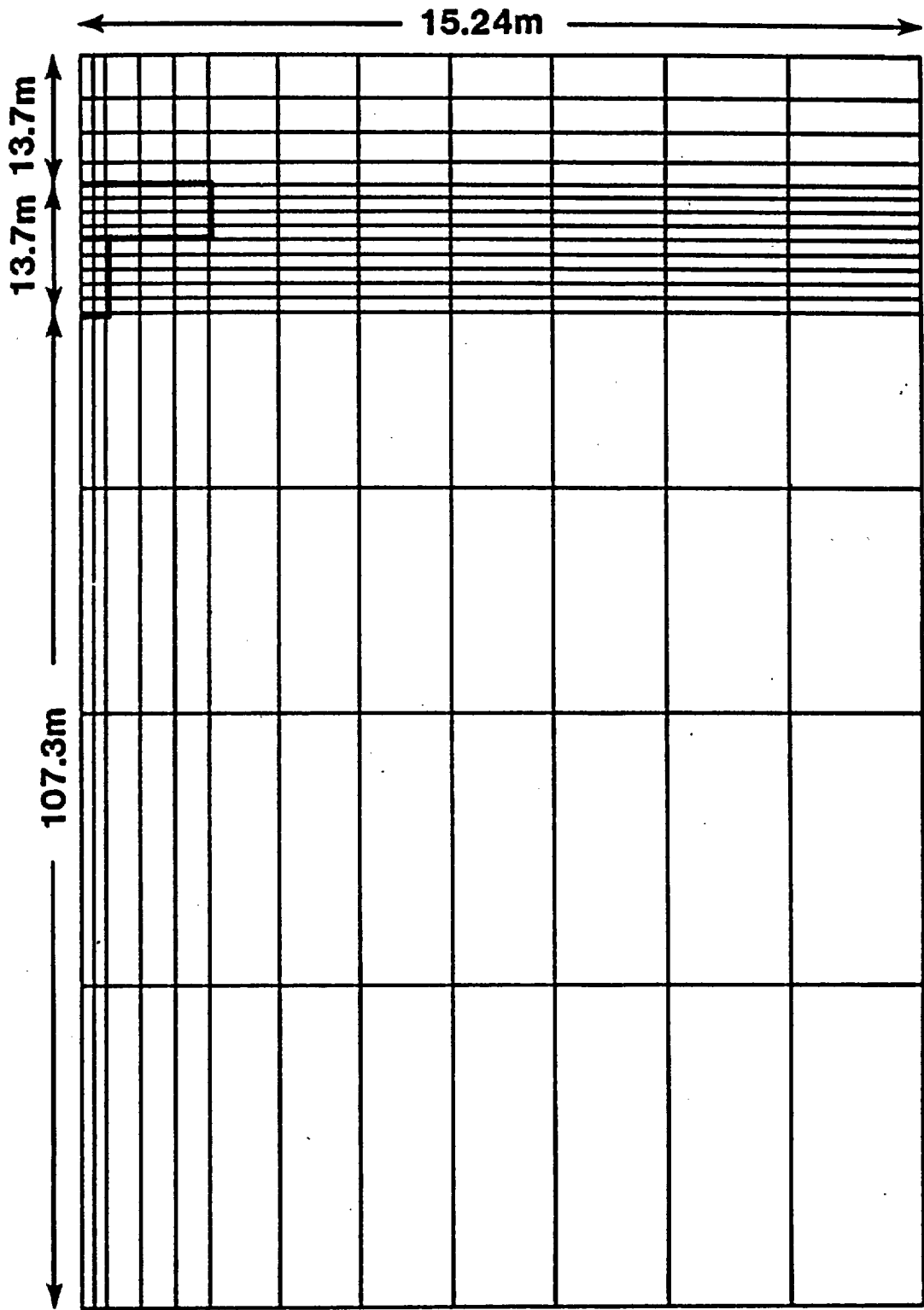


Figure 2. Finite-element mesh with drift and waste package outlined in bold (not to scale -- horizontal axis has been stretched to show detail).

condition at the lower boundary. For example, if the bottom surface is the water table, this lower boundary condition implies that the water table does not rise as it rains. The pressure at the bottom of the mesh is chosen so that at hydrostatic conditions (uniform effective pressure), the tuff has an initial saturation of 86% at drift level [4].

The left boundary is a plane of symmetry. The right boundary is also a plane of symmetry, if we model a drift in the interior of the repository. Therefore, the width of the model is half the distance between drifts. The upper and lower boundaries are sufficiently far from the drift so that they do not influence the flow near the drift. We assume steady state is reached when the moisture front is well below the waste package and a material balance on the drift shows no accumulation or depletion of water.

3. MATERIAL PROPERTIES AND INITIAL CONDITIONS

The material properties for the tuff, sand, clay and water used in the SAGUARO simulations are listed in Table 1.

TABLE 1.
MATERIAL PROPERTIES

Material Property	Value		Reference
Density of Water	1000.	kg/m ³	[5]
Viscosity of Water	9.82×10^{-4}	Pa-s	[5]
Saturated Permeability of Tuff (USW GU-3, Sample S-19 at 1730 ft depth)	1.21×10^{-16}	m ²	[7]
Saturated Permeability of Clay (Chino clay)	3.92×10^{-16}	m ²	[6]
Saturated Permeability of Sand (Crab Creek sand)	1.93×10^{-13}	m ²	[6]
Porosity of Tuff ϕ (USW GU-3, Sample S-19 at 1730 ft depth)	0.221		[7]
Porosity of Clay ϕ (Chino clay)	0.532		[6]
Porosity of Sand ϕ (Crab Creek sand)	0.371		[6]

In unsaturated zones, the permeability and saturation are strongly dependent upon the pressure head. For the analysis reported here, the hydrologic relationships for tuff, clay, and sand necessary for implementing SAGUARO are represented by the curves in Figures 3 through 7. Each material has three characteristic curves relating the permeability k_{ij} , the moisture content θ , and the storage capacity C ($\partial\theta / \partial\psi$) to the pressure head ψ . SAGUARO actually requires input of the moisture content in terms of saturation, where $\theta_s = \theta/\phi$; hence, these figures show the relationships between saturation and pressure head. We assume all materials are isotropic in terms of permeability (ie., $k_{ij} = k_{ji}$). The curves for the permeability and

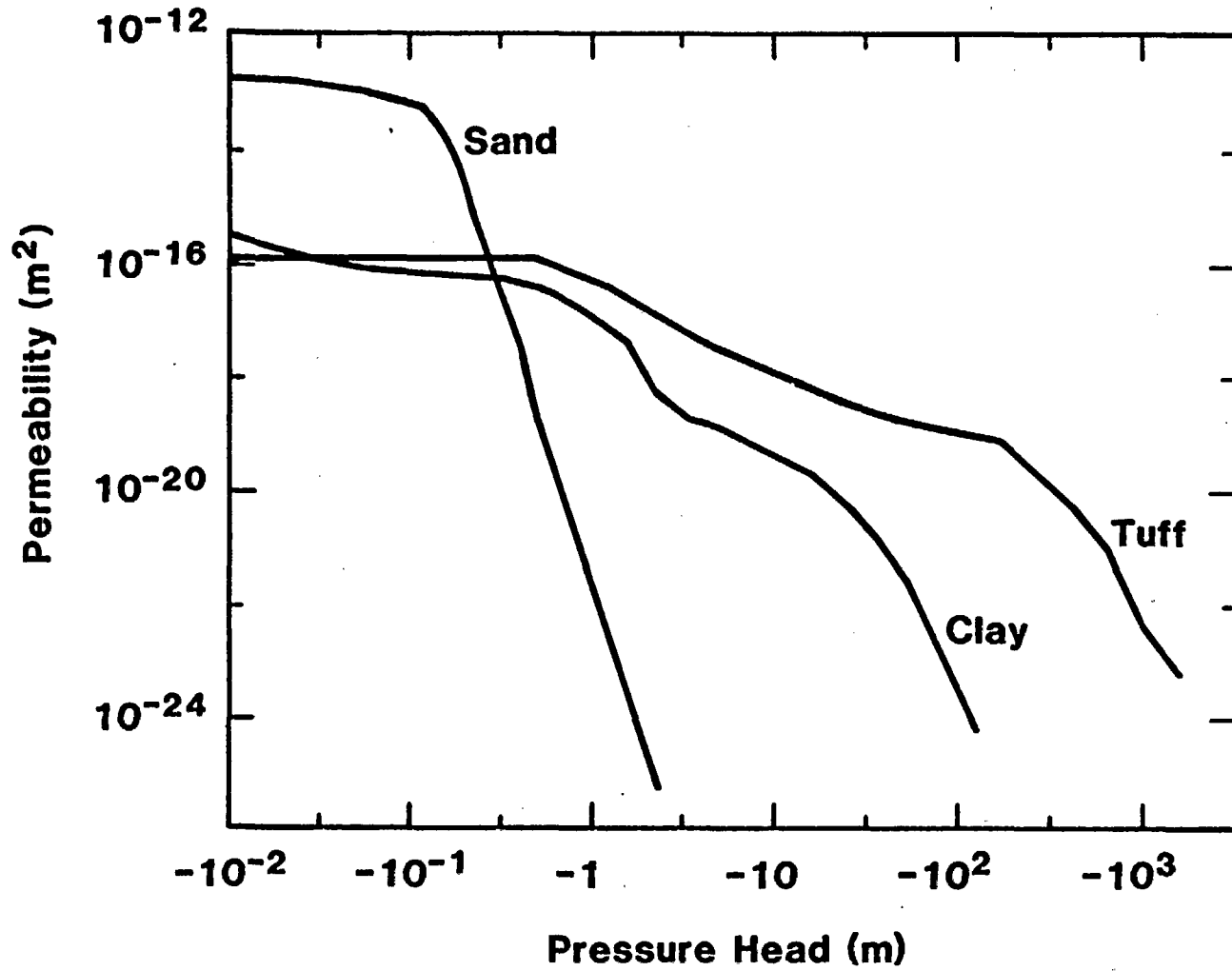


Figure 3. Permeability vs pressure head -- characteristic curves for tuff, clay, and sand.

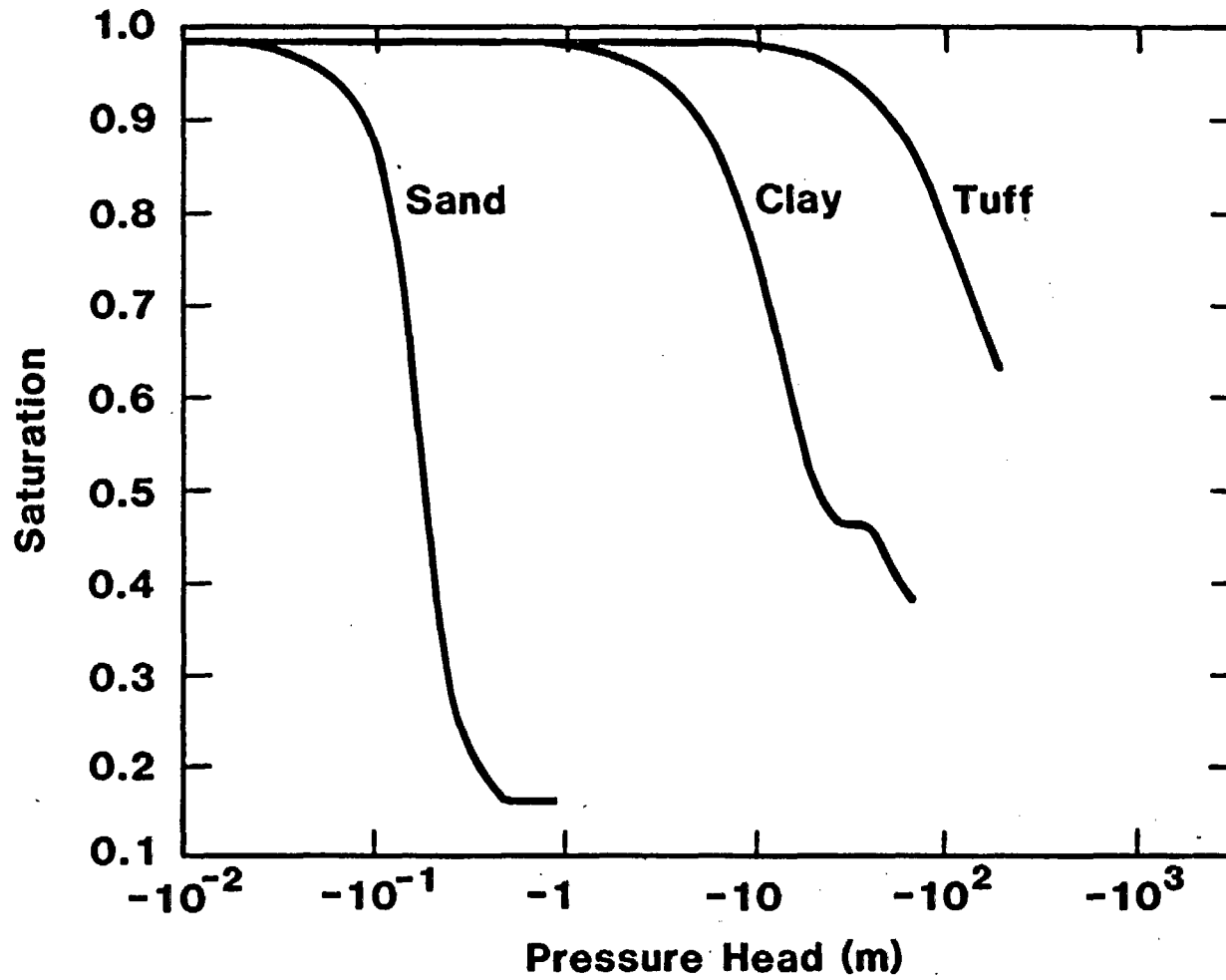


Figure 4. Saturation vs pressure head -- characteristic curves for tuff, clay, and sand (Note that the kink in the curve for clay is an artifact of the spline fit used and that it is not in the pressure range of interest).

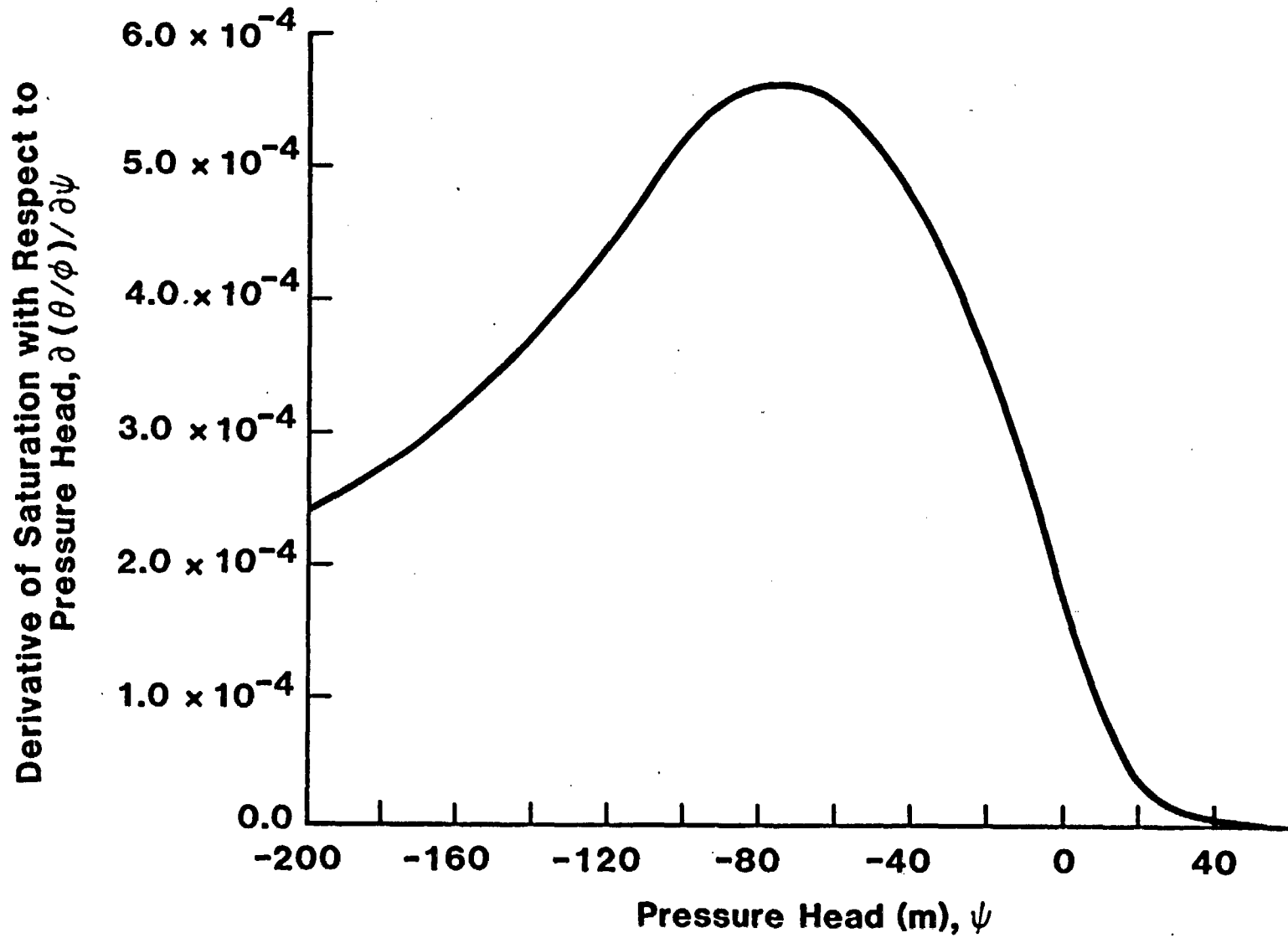


Figure 5. Derivative of saturation with respect to pressure head -- characteristic curve for tuff.

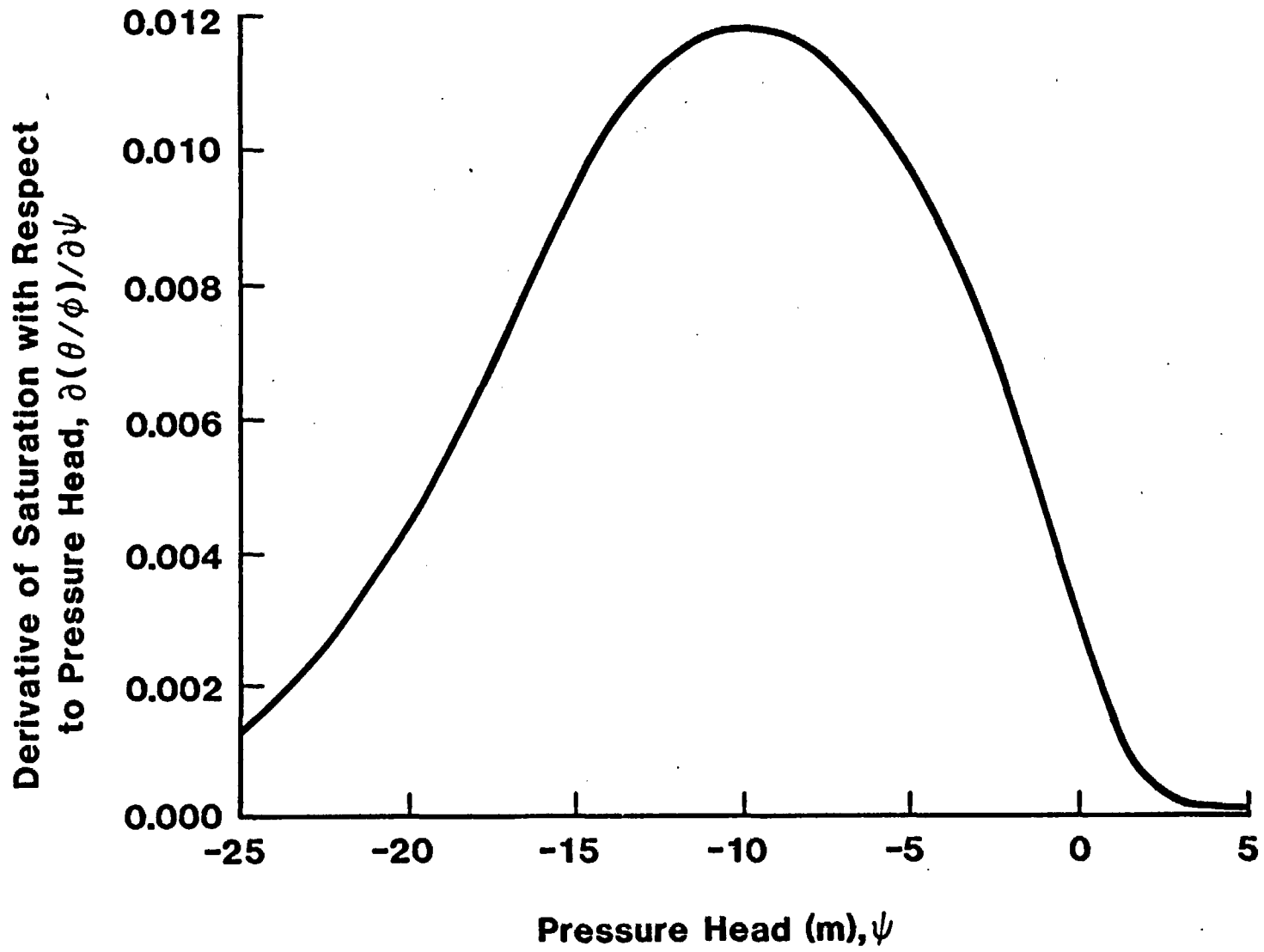


Figure 6. Derivative of saturation with respect to pressure head -- characteristic curve for clay.

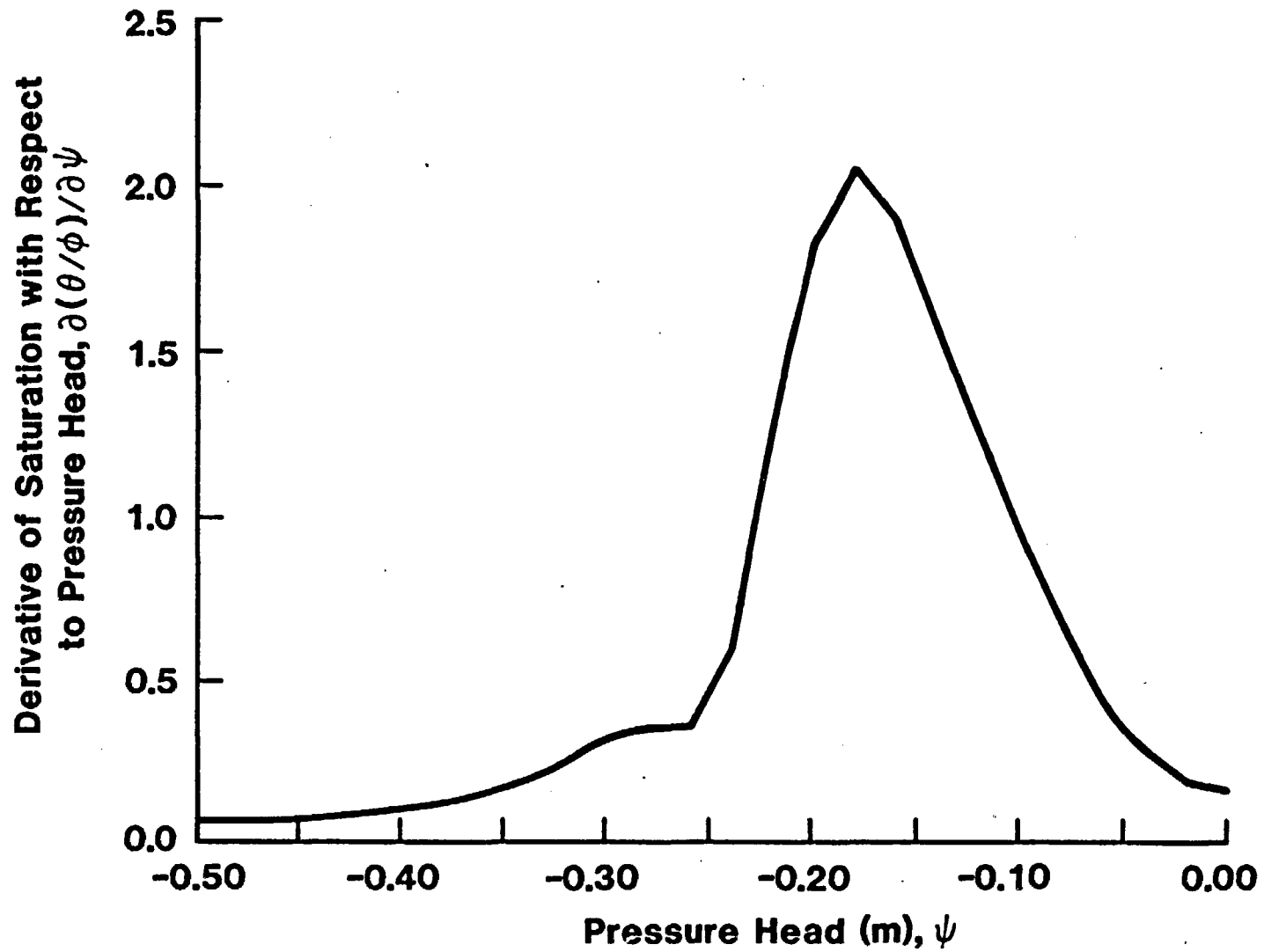


Figure 7. Derivative of saturation with respect to pressure head -- characteristic curve for sand.

data points using a standard library spline routine [8]. In all cases, the curves for the derivative of saturation (Figures 5 through 7) are calculated numerically using the same spline routine.

Notice that the permeabilities of two different materials at the same pressure head can vary over several orders of magnitude (Figure 3). Notice, also, that the permeability of a single material can vary over several orders of magnitude with very little change in head. When modeling a region of clay or sand backfill immediately adjacent to an area of tuff, we place a sharp discontinuity in the permeability at the boundary of the two regions. This is especially true when placing sand adjacent to tuff.

The steepness of the permeability curve of sand can lead to numerical instabilities. At each time step, a solution to the pressure field is obtained through iteration. If the calculated pressure changes a small amount between iterations, the flow changes dramatically, making convergence of Richards equation difficult and the calculated velocities unrealistic. Several minor modifications to the code and element grid can help overcome this problem, and these will be discussed in the next section. However, because of limits on computer time and storage, we elect to modify the assumed characteristic permeability curve of sand. Therefore, we arbitrarily assume that below a permeability of $2.2 \times 10^{-19} \text{ m}^2$, the logarithm of the permeability function varies linearly with the logarithm of the pressure head, as illustrated with the dotted line in Figure 8. This modified function ensures that the assumed permeability of sand is always at least three orders of magnitude below that of the tuff (at the same suction head), while allowing computational convergence to occur.

SAGUARO sets the initial effective pressure (ϕ) equal everywhere for each material; in other words, each material is in hydraulic equilibrium within itself but not necessarily with surrounding materials. Therefore, the initial pressure head (ψ), and hence the initial saturations, are not uniform throughout the element mesh, but vary with height. We set the initial saturation at the height of the midpoint of the drift to be the initial average saturations for sand and clay, chosen by PNL as possible water contents necessary for packing. These saturations set at the midpoint (0.86, 0.72, and 0.64 for tuff, clay and sand, respectively) lead to the initial saturations as a function of height, listed in Table 2.

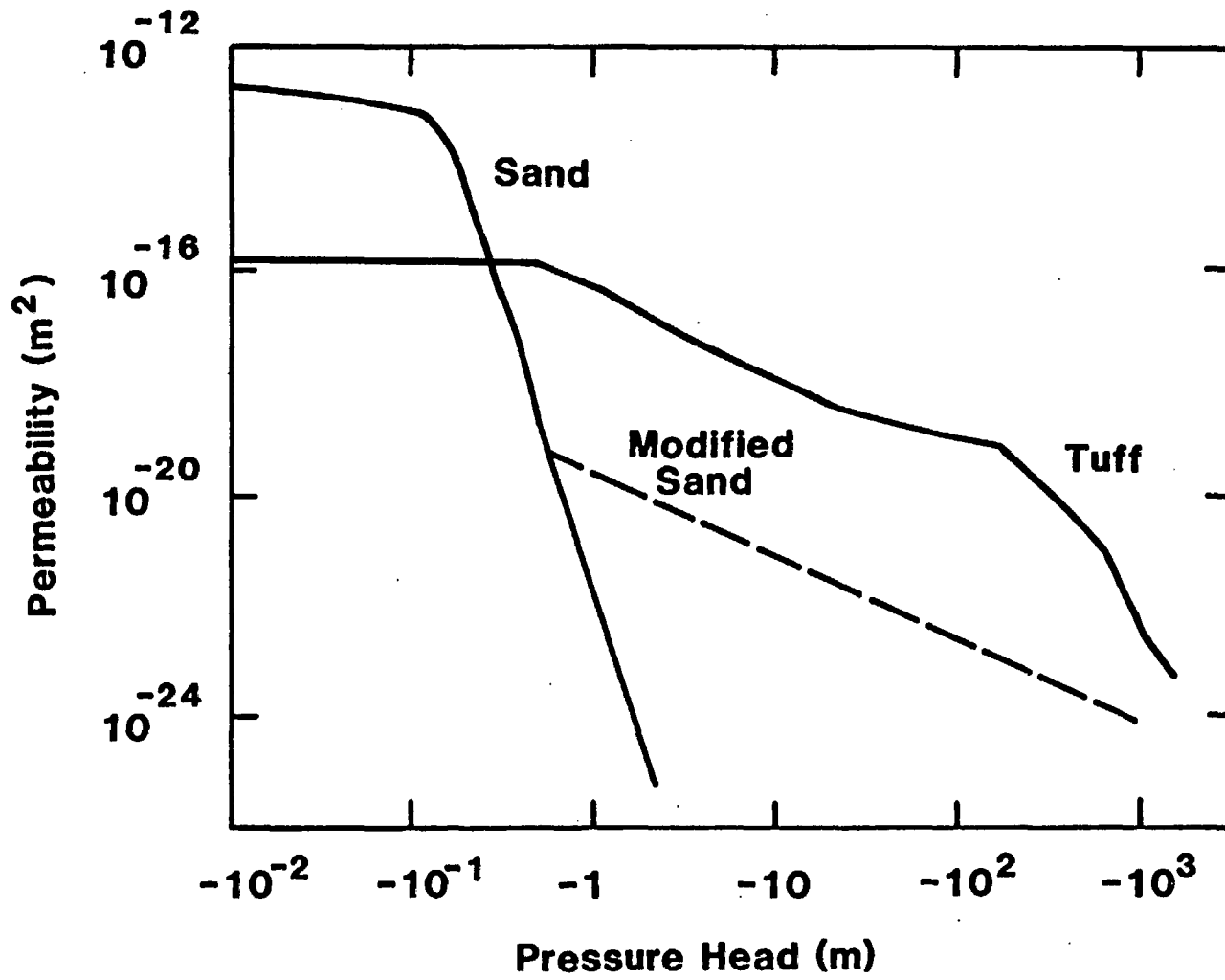


Figure 8. Modified permeability characteristic curve for sand.

TABLE 2.
INITIAL SATURATION CONDITIONS

Level	Tuff	Clay	Sand
Top of Mesh	0.82	----	----
Top of Drift	0.85	0.63	0
Bottom of Drift	0.87	0.81	1.0
Midpoint of Canister	0.88	----	----
Bottom of Mesh	0.92	----	----

Note that the sand ranges from unsaturated to saturated over the height of the drift (at the midpoint of the drift the saturation is set at .64, as mentioned above). The clay and tuff have characteristic curves which vary more slowly with head, and, therefore, their saturations differ less than the saturation of sand with height.

4. NUMERICAL INSTABILITIES WHEN MODELING SAND

As mentioned above, the steep gradients of the characteristic curves of sand can cause numerical difficulties. The finite-element method employed suggests three different approaches to cope with these difficulties: the mesh can be made finer, the time steps smaller, and the iteration criterion tighter. Each of these procedures results in an increase in the computer time required to reach a solution. We feel that refining the mesh is the least effective way to overcome the numerical instabilities, because the sand permeability (Figure 3) can change over seven orders of magnitude with a change of 0.1 m in pressure head, and because the number of elements allowed in SAGUARO is limited to one thousand. Shortening the time steps helps improve the stability of the numerical solution; however, the computer time increases prohibitively. Tightening the convergence criterion (decreasing the allowed difference between iterations in the calculated effective pressure) results in excessive time spent in iterating. If the pressure changes too drastically in one time step, the convergence criterion may not be met at all.

Another procedure, using an adaptive time step coupled to the number of iterations required to meet the convergence criterion, saves considerable computational time [9]. This procedure allows larger time steps to be taken in intervals of slowly changing permeability and specific moisture content, but automatically reduces the time step when a more difficult solution interval is encountered. We specify a convergence tolerance (ϵ) and a maximum number of iterations. SAGUARO then iterates until the normalized difference in effective pressure ($\Delta\phi/\phi$) between iterations is less than ϵ , or the number of iterations in the time plane is greater than the maximum specified. If the latter is the case, the time is backed up to the last solution reached, the time step automatically reduced, the time advanced by the smaller step size and the solution attempted again. If convergence is achieved, the time step is increased by a specified percentage. Often we approach convergence alternately from both sides of an asymptote. Therefore, the convergence criterion is based on the average pressure value of successive iterations rather than on the last value.

These modifications help stabilize the solution; however, the sand curve must be modified to be less steep. Since the main goal of this modeling effort is to compare the effects of various backfill materials in the drift on the flow-rate past the waste package, a major change in the assumed permeability of the sand backfill can affect the conclusions. From comparing the permeability of tuff and sand, we expect that the sand will behave as though it were impermeable. In a separate simulation to test this hypothesis, we have modeled the drift as an impermeable zone. Using pressure information obtained with this approximation, we can predict the flow behavior if the true sand properties were included in the model. If indeed it appears that the sand will approximate an impermeable material, the two sets of velocities calculated with the two different drift models can be compared to ensure that the modified permeability of sand is a valid approximation at the steady-state conditions. Note that although modeling sand as an impermeable material leads to no numerical difficulties, it cannot predict the behavior of sand in higher saturation regimes where the sand can become much more permeable than the surrounding host rock. It is desirable to be able to estimate the behavior of sand using characteristic curves that will give physically correct solutions if the sand is saturated (especially because part of the drift is assumed to be saturated initially).

The pressure head at the drift boundary increases as the permeability difference across the boundary increases, reaching a maximum if the drift is impermeable. By looking at the pressure head, calculated for an impermeable drift, and taking it as the maximum that could exist, one can argue that a negligible amount of moisture will infiltrate a sand-filled drift considering the permeabilities of sand and tuff at this pressure. The pressure head calculated at the impermeable drift boundary is less than -1.5 m. From the permeability versus pressure curves in Figure 3, the permeability of tuff (k_t) at -1.5 m is approximately $1 \times 10^{-16} \text{ m}^2$, whereas the permeability of sand (k_s) is about $1 \times 10^{-22} \text{ m}^2$. The sharp disparity between the permeabilities across the interface indicates that sand in the drift would allow negligible flow.

Using the effective pressure seen across the impermeable drift (again the maximum that could occur), we can also estimate the velocities that might occur in a sand-filled drift. With steady, one-dimensional flow, Richards equation reduces to:

$$v = - \frac{k}{\mu} \frac{\partial \phi}{\partial x} = \text{constant} \quad (3)$$

We can calculate the velocity (v) in the sand due to the effective pressure drop across the entire drift. The necessary parameters are:

$$\begin{aligned} k_s &= 1 \times 10^{-22} \text{ m}^2, \\ \mu &= 1 \times 10^{-3} \text{ Pa-s}, \\ \Delta x &= 6 \text{ m}, \\ \text{and } \Delta \phi &= 1 \times 10^5 \text{ Pa}. \end{aligned}$$

Therefore, v is approximately 1.7×10^{-15} m/s downward. This velocity is very small compared to the velocity in the tuff of about 1.3×10^{-10} m/s, indicating that an extremely small fraction of the influx would travel through the drift. In the Results section, we compare the velocities near the waste package calculated with the two drift models.

The velocities calculated by SAGUARO have an inherent error bar associated with them. The iteration criterion used in these simulations is $\epsilon = (\Delta \phi / \phi)_{\text{max}} = 0.0006$. With the steady-state value for ϕ , and at the level midway between the drift and the bottom of the waste package, this criterion gives $\Delta \psi = 0.06$ m in the tuff. In the center of the sand-drift, it gives $\Delta \psi = 0.07$ m. At the final conditions, this translates into an allowed variation in permeability of the tuff and modified sand of about $\pm 4\%$. At steady state the velocities are directly proportional to the permeability. Hence, the velocities can vary within an 8% band due to changes in permeability only. A changing pressure at one point can cause the gradient of pressure with distance to change also. This variation of pressure gradient multiplied by the variation in permeability leads to an even greater percentage of uncertainty in velocity. We estimate this uncertainty to be about 12%.

The gridding can also cause instabilities, although these are less well understood. In order to extend the grid far below the area of interest, we allowed a large jump in element size immediately below the canister. The velocities along this boundary vary cyclically in time and with somewhat greater changes in amplitude than the velocities elsewhere.

5. RESULTS

Figures 9 through 11 depict contours of constant effective pressure (equipotentials) at various times when groundwater is flowing downward toward a drift filled with clay (flow paths lie perpendicular to the equipotentials). Flow begins immediately outward from the drift, because the clay is initially at a higher effective pressure. As water enters from the top of the mesh, a pressure front propagates downward, eventually encountering the circular push from the drift. In the Figure 11 the front has passed the drift and waste package. This last figure shows the steady-state equipotentials in the vicinity of the drift and waste package. Note that the drift does not cause significant disturbance to the downward flow. The infiltration process is not rapid; Figure 11 is 600 years after time zero. Not only are we essentially assuming that the infiltration rate is constant over hundreds of years, but we are setting the tuff to be initially at hydrostatic conditions and the infiltration to begin at time equals zero. Hence, this early time behavior is of qualitative interest only. The sequence of events of a sand-filled drift is similar to that of the drift filled with clay; although the water is deflected more dramatically away from the drift. Note that at steady state (Figure 12), the drift disturbs the downward flow significantly only very near the drift (within about one drift width), even when no flow is allowed through the drift.

Steady state in the region of the drift is achieved within 600 years, when the drift moisture content no longer is changing and the pressure front is well past the depth of the waste package. The final conditions are outlined in Table 3. The steady-state saturation of the sand (with the modified permeability) ranges from approximately 0.17 to the residual saturation (-0.15). Note that the sand-filled drift drains so that its final saturation is much lower than the initial average saturation. This is in contrast to the water absorption by a clay-filled drift. The clay has a final saturation of 0.90 to 0.98, whereas its initial saturation was lower than 0.81.

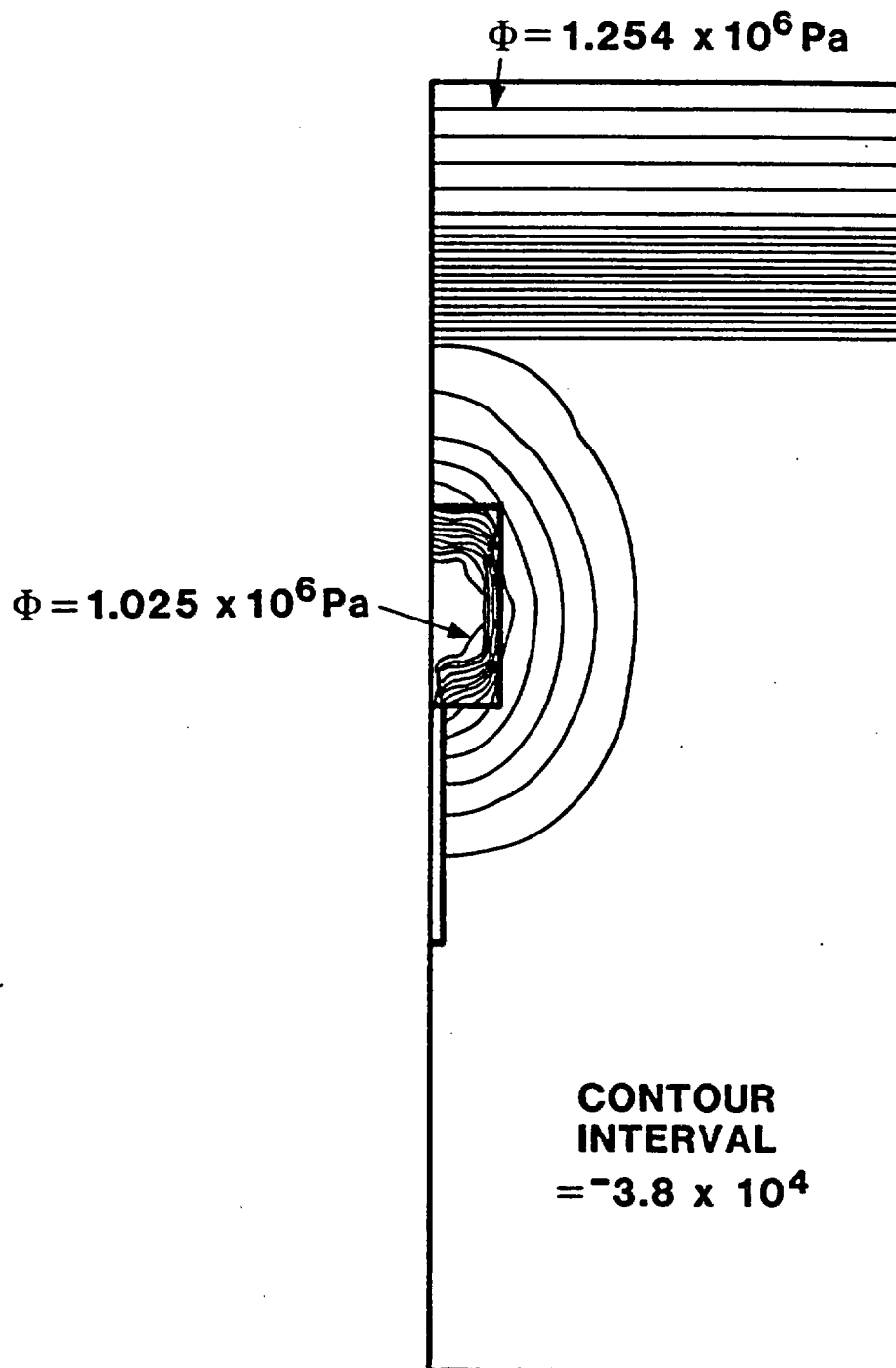


Figure 9. Contours of constant effective pressure at time = 50 years for a clay-filled drift.

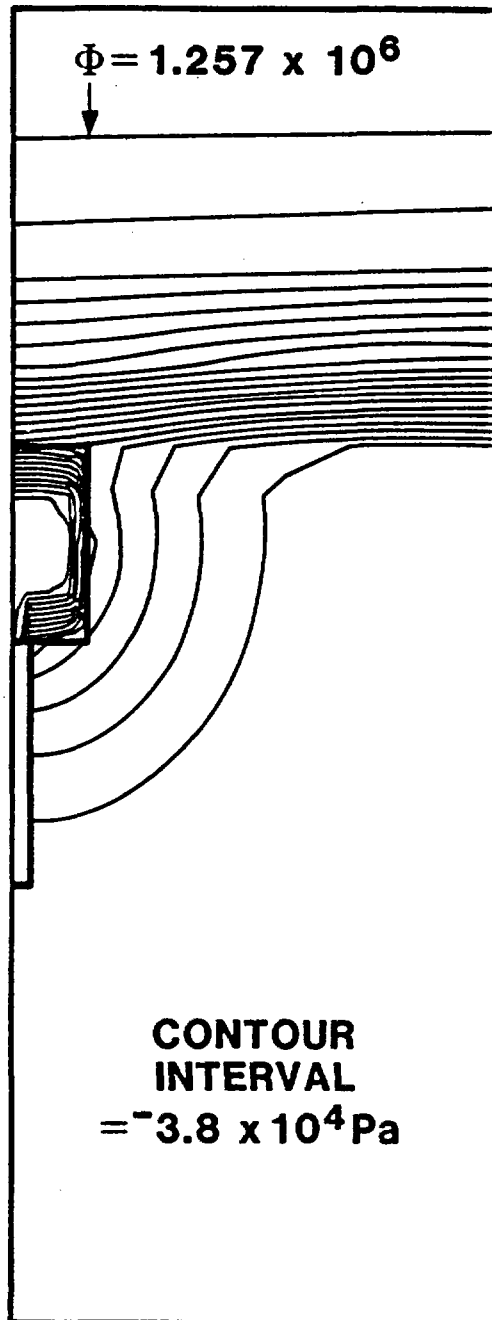
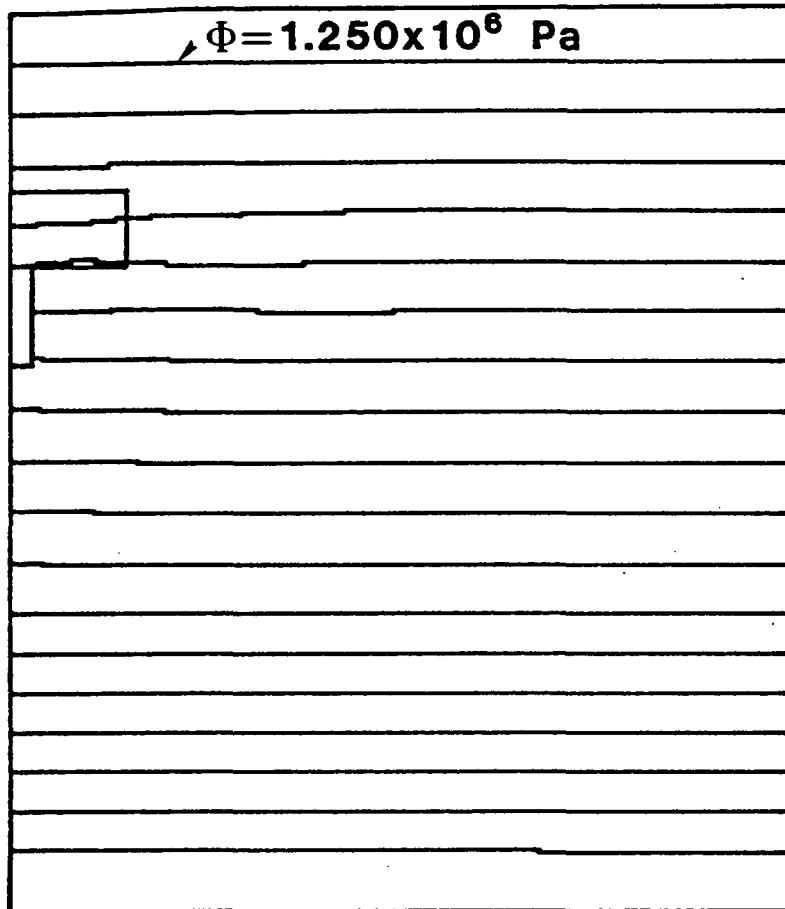
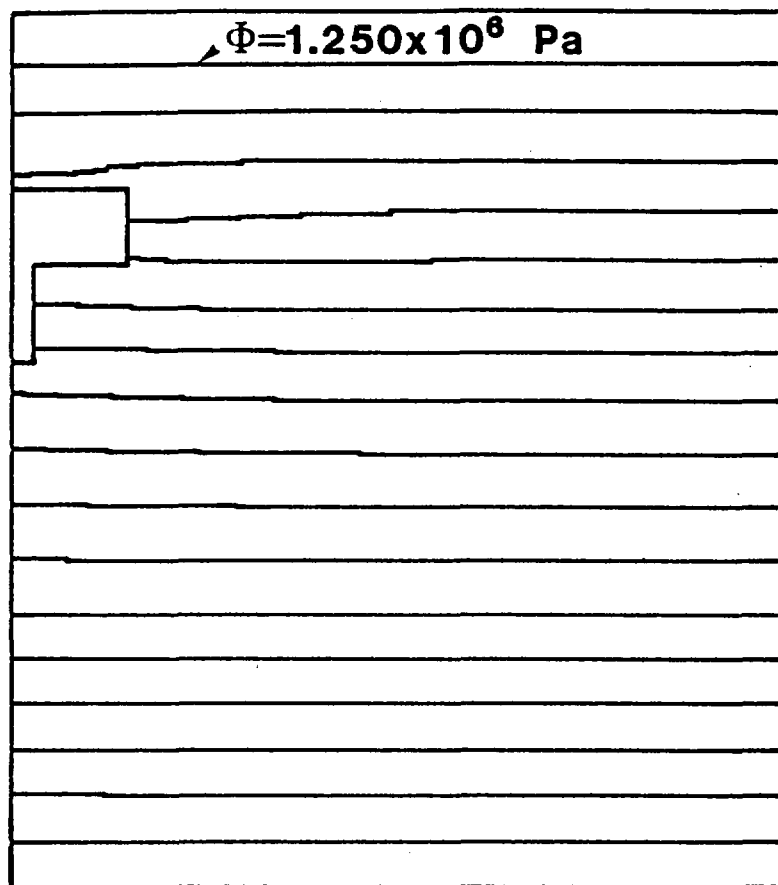


Figure 10. Contours of constant effective pressure at time = 109 years for a clay-filled drift.



CONTOUR INTERVAL = $-3.8 \times 10^4 \text{ Pa}$

Figure 11. Contours of constant effective pressure at time = 600 years (steady state) for a clay-filled drift (not to scale -- horizontal axis has been stretched to show detail).



CONTOUR INTERVAL = -3.6×10^4 Pa

Figure 12. Contours of constant effective pressure at time = 600 years for an impermeable drift (not to scale -- horizontal axis has been stretched to show detail).

TABLE 3.
 STEADY-STATE CONDITIONS
 (Infiltration rate = 0.4 cm/yr = 1.097×10^{-5} m/day)

Fill Material	Condition	
Clay	Saturation Range of Tuff	0.92 - 0.99
Clay	Saturation Range of Fill	0.90 - 0.98
Sand (modified permeability)	Saturation Range of Tuff	0.92 - 0.99
Sand (modified permeability)	Saturation Range of Fill	0.17 - residual
Clay	Flux Through the Drift	$4.5 \times 10^{-5} \text{ m}^3/\text{m depth/day}$
Sand (impermeable)	Flux Through the Drift	$0 \text{ m}^3/\text{m depth/day}$

The flow-rates listed here are gross flow-rates through the entire drift (only half the drift is actually modeled due to symmetry).

Once steady state near the waste package has been reached, quantitative values of flow-rates through the drift and past the waste package are of interest. Recall that the floor emplacement drift is assumed to be 4.57 m (15 ft) wide and 6.1 m (20 ft) high (see Figure 1). The flow-rates listed in Table 3 are gross flow-rates through the entire drift (only half the drift is actually modeled due to symmetry). The flow-rate through the clay drift overestimates the flux that would actually occur, because the velocities calculated at the boundary of the drift and surrounding tuff reflect the higher permeability of the tuff. This will be discussed in detail in the following paragraphs. Because we have modified the sand's permeability, the calculated velocities using this approximation overestimate the flow through the drift perhaps by several orders of magnitude. If sand is modeled as impermeable, obviously no flow is allowed through the drift. From arguments detailed in Section 4, the flow through a sand-filled drift is very likely to be close to zero.

In Tables 4 through 6, the flows between individual elements in and near a clay-filled drift are listed. Figure 13 is a blow-up of the area of interest, with the elements numbered for reference. The velocities are averaged along the line shared by two adjacent elements and, therefore, represent the component of velocity from the center of one element to the center of the next element.

TABLE 4.
STEADY-STATE FLOW THROUGH THE CLAY-FILLED DRIFT

Element		Length Scale of Element x Unit Thickness (m ²)	Fluid Flow	
from	to		Velocity (m/day)	Volumetric Flow (m ³ /day)
Flow Into Drift				
14	13	0.229	9.504 x 10 ⁻⁶	2.176 x 10 ⁻⁶
31	30	0.229	9.461 x 10 ⁻⁶	2.167 x 10 ⁻⁶
48	47	0.61	9.331 x 10 ⁻⁶	5.692 x 10 ⁻⁶
65	64	0.61	9.072 x 10 ⁻⁶	5.534 x 10 ⁻⁶
82	81	0.61	1.045 x 10 ⁻⁵	6.377 x 10 ⁻⁶
95	78	1.524	3.888 x 10 ⁻⁷	5.925 x 10 ⁻⁷
Flow Out Drift				
81	98	1.524	2.678 x 10 ⁻⁶	4.082 x 10 ⁻⁶
80	97	1.524	1.650 x 10 ⁻⁶	2.515 x 10 ⁻⁶
79	96	1.524	1.218 x 10 ⁻⁶	1.857 x 10 ⁻⁶
78	77	0.61	8.001 x 10 ⁻⁶	4.880 x 10 ⁻⁶
61	60	0.61	4.856 x 10 ⁻⁶	2.962 x 10 ⁻⁶
44	43	0.61	5.599 x 10 ⁻⁶	3.415 x 10 ⁻⁶
27*	26	0.229	5.936 x 10 ⁻⁶	1.359 x 10 ⁻⁶
10*	9	0.229	5.944 x 10 ⁻⁶	1.361 x 10 ⁻⁶
Overall in (1/2 DRIFT)				2.254 x 10 ⁻⁵
Overall out (1/2 DRIFT)				2.243 x 10 ⁻⁵

*Flow from elements 10 and 27 to the impermeable zone below is due to the averaging of effective pressure gradients and permeabilities.

Note that the representative velocities inside the drift are lower than those on the perimeter. This is partly because the velocities are calculated from Richards equation (1), and the effective pressure gradients and permeabilities calculated across this boundary between materials reflect

14	31	48	65	82	99
13	30	47	64	81	98
12	29	46	63	80	97
11	28	45	62	79	96
10	27	44	61	78	95
9	26	43	60	77	94
8	25	42	59	76	93
7	24	41	58	75	92
6	23	40	57	74	91
5	22	39	56	73	90

Figure 13. Close-up of the finite-element mesh in the vicinity of the drift and waste package.

TABLE 5.
STEADY-STATE FLOW INSIDE CLAY-FILLED DRIFT

Element		Length Scale of Element x Unit Thickness (m ²)	Fluid Flow	
from	to		Velocity (m/day)	Volumetric Flow (m ³ /day)
Flow Toward Center of Drift (in)				
13	12	0.229	7.577×10^{-6}	1.735×10^{-6}
30	29	0.229	7.443×10^{-6}	1.705×10^{-6}
47	46	0.61	7.011×10^{-6}	4.277×10^{-6}
64	63	0.61	5.905×10^{-6}	3.602×10^{-6}
Flow away from Center of Drift (out)				
11	10	0.229	6.130×10^{-6}	1.404×10^{-6}
28	27	0.229	5.456×10^{-6}	1.249×10^{-6}
45	44	0.61	4.739×10^{-6}	2.891×10^{-6}
62	61	0.61	3.992×10^{-6}	2.435×10^{-6}
63	80	1.524	1.205×10^{-6}	1.837×10^{-6}
62	79	1.524	1.002×10^{-6}	1.527×10^{-6}

the higher transmissivity of the tuff. However, one point to note from the tables above and Table 6 is that the steady-state permeabilities found inside the clay drift are not considerably smaller than those in the surrounding tuff, and consequently the velocities in the two materials are often within an order of magnitude of each other.

Flow from elements 10 and 27 to the impermeable zone below is due to the averaging of pressure gradients and permeabilities. Also a small amount of flow at the impermeable side boundaries is allowed because of the approximate (quadratic) form of the pressure profile used to calculate the velocities. The materials we are modeling are so impermeable as to allow flow only one or two orders of magnitude higher than this "residual" flow. This affects the material balance obtained in the third significant figure of the overall volumetric flow.

Table 6 lists the velocities under a clay-filled drift. The third column in Table 6 is the fraction of the prescribed influx seen along the canister; in other words, it is the calculated velocity divided by 1.097×10^{-5} m/day.

TABLE 6.
VELOCITIES IN TUFF NEAR DRIFT AND WASTE PACKAGE

Element from	to	Velocity (m/day)	Fraction of Influx Flow (VELOCITY/1.097x10 ⁻⁵)
Vertical Connections			
43	42	8.104 x 10 ⁻⁶	0.74
42	41	9.245 x 10 ⁻⁶	0.84
41	40	9.936 x 10 ⁻⁶	0.91
40	39	1.037 x 10 ⁻⁵	0.95
39	38	1.054 x 10 ⁻⁵	0.96
60	59	8.225 x 10 ⁻⁶	0.75
59	58	9.504 x 10 ⁻⁶	0.87
58	57	1.011 x 10 ⁻⁵	0.92
57	56	1.045 x 10 ⁻⁵	0.95
56	55	1.084 x 10 ⁻⁵	0.99
77	76	9.547 x 10 ⁻⁶	0.87
76	75	1.011 x 10 ⁻⁵	0.92
75	74	1.045 x 10 ⁻⁵	0.95
74	73	1.067 x 10 ⁻⁵	0.97
73	72	1.115 x 10 ⁻⁵	1.02
92	91	1.098 x 10 ⁻⁵	1.00
91	90	1.098 x 10 ⁻⁵	1.00
Horizontal Connections			
94	77	1.840 x 10 ⁻⁶	
77	60	1.127 x 10 ⁻⁶	
60	43	5.184 x 10 ⁻⁸	
93	76	1.331 x 10 ⁻⁶	
76	59	8.755 x 10 ⁻⁷	
59	42	3.974 x 10 ⁻⁷	
92	75	7.171 x 10 ⁻⁷	
75	58	5.541 x 10 ⁻⁷	
58	41	2.851 x 10 ⁻⁷	
91	74	4.795 x 10 ⁻⁷	
74	57	3.697 x 10 ⁻⁷	
57	40	2.030 x 10 ⁻⁷	
90	73	3.456 x 10 ⁻⁷	
73	56	3.219 x 10 ⁻⁷	
56	39	2.722 x 10 ⁻⁷	

Part of the fluid is flowing around the drift, and, therefore, the gross flow under the drift has a vector component toward the canister. The water traveling through the drift is flowing horizontally out from the drift symmetry plane (especially near the center where it must detour around the impermeable region directly below). These two flows meet at element 43 and account for the very small magnitude of the horizontal flow there. Element 91 is located at the level of the center of the waste package and to the right of the drift above. The velocity in this element is very close (differs by less than 1%) to that prescribed at the top boundary, indicating that the drift does not affect the flow-rate at the waste package level much beyond the width of the drift. Even the flow in the elements immediately adjacent to the waste package is 91% to 96% of the influx rate. The velocities for elements in the vicinity of a waste package below a sand-filled drift are listed in Tables 7 and 8. Table 7 contains the velocities calculated when sand with modified permeability is in the drift. The third column in Table 7 is the calculated velocity divided by 1.097×10^{-5} m/day. The last column in the table is the velocity, when sand is in the drift, divided by the velocity when clay is the backfill.

The vertical flow in the elements immediately adjacent to the waste package is 81% to 92% of the influx rate. This indicates that the drift influences the flow past the waste package somewhat. Because the drift has a low permeability, most of the fluid must flow around it. The gross flow under the drift, therefore, has a component of velocity toward the waste package. Because more water is forced around the sand-filled drift than is deflected when the drift is filled with clay, the horizontal component under a sand-filled drift is larger than that under a clay-filled drift. Recall that with the clay as a backfill, the horizontal component of flow is small near the interface of the drift and the impermeable waste package, where the water traveling through the drift meets the water flowing under the drift. With sand in the drift, there is very little flow through the drift to meet with the flow around it.

Listed in Table 8 are the values of the velocities calculated when the drift is assumed to be completely impermeable. The last column is the ratio of the velocities calculated when the drift is impermeable to the velocities calculated when the drift is filled with a sand with the modified permeability curve.

TABLE 7.
VELOCITIES IN TUFF NEAR DRIFT AND WASTE PACKAGE
WITH A SAND-FILLED DRIFT

Element from to	Velocity (m/day)	Fraction of Influx Flow	Fraction of Flow with Clay Fill
Vertical Connections			
42 41	7.47×10^{-6}	0.68	0.81
41 40	8.90×10^{-6}	0.81	0.90
40 39	9.63×10^{-6}	0.88	0.93
39 38	10.15×10^{-6}	0.92	0.96
59 58	7.99×10^{-6}	0.73	0.84
58 57	9.20×10^{-6}	0.84	0.91
57 56	9.81×10^{-6}	0.89	0.94
56 55	10.45×10^{-6}	0.95	0.96
76 75	9.20×10^{-6}	0.84	0.91
75 74	9.85×10^{-6}	0.90	0.94
74 73	10.20×10^{-6}	0.93	0.96
73 72	10.80×10^{-6}	0.98	0.97
Horizontal Connections			
93 76	2.44×10^{-6}		1.83
76 59	2.10×10^{-6}		2.40
59 42	1.11×10^{-6}		2.79
92 75	1.39×10^{-6}		1.94
75 58	1.08×10^{-6}		1.95
58 41	0.59×10^{-6}		2.08
91 74	0.91×10^{-6}		1.91
74 57	0.68×10^{-6}		1.85
57 40	0.38×10^{-6}		1.86
90 73	0.58×10^{-6}		1.68
73 56	0.48×10^{-6}		1.50
56 39	0.36×10^{-6}		1.32

TABLE 8.
VELOCITIES IN TUFF NEAR DRIFT AND WASTE PACKAGE
WITH AN IMPERMEABLE DRIFT

Element from to	Velocity (m/day)	Fraction of Flow with Sand Fill
Vertical Connections		
42 41	7.47×10^{-6}	1.00
41 40	8.73×10^{-6}	0.98
40 39	9.37×10^{-6}	0.97
39 38	9.85×10^{-6}	0.97
59 58	7.99×10^{-6}	1.00
58 57	9.03×10^{-6}	0.98
57 56	9.55×10^{-6}	0.97
56 55	10.20×10^{-6}	0.98
76 75	9.24×10^{-6}	1.00
75 74	9.72×10^{-6}	0.99
74 73	9.94×10^{-6}	0.98
73 72	10.60×10^{-6}	0.98
Horizontal Connections		
93 76	2.50×10^{-6}	1.02
76 59	2.15×10^{-6}	1.02
59 42	1.15×10^{-6}	1.04
92 75	1.40×10^{-6}	1.01
75 58	1.10×10^{-6}	1.02
58 41	0.60×10^{-6}	1.02
91 74	0.89×10^{-6}	0.98
74 57	0.67×10^{-6}	0.99
57 40	0.37×10^{-6}	0.98
90 73	0.51×10^{-6}	0.88
73 56	0.43×10^{-6}	0.90
56 39	0.32×10^{-6}	0.90

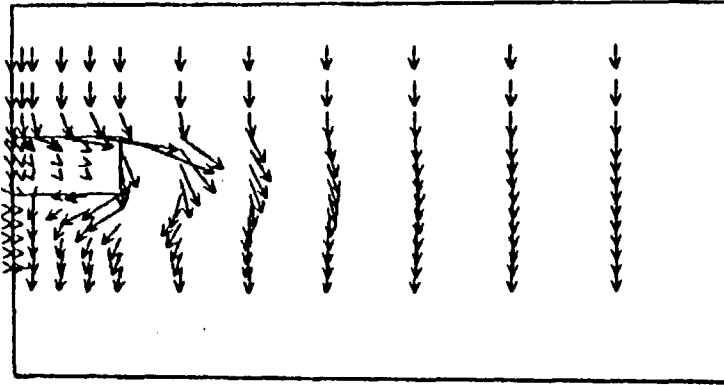
The velocities near the canister when the drift is assumed to be impermeable are very close in value to those calculated when the drift is filled with sand. The velocities very near the drift, however, differ between the two approximations. As mentioned above, the impermeable drift allows no water to pass through, whereas the modified curve allows more flow than would the true sand curve. Consequently, more flow is forced along the

top of the drift and out to the side with the impermeable approximation to the sand. The general nature of the flow is illustrated for the modified permeability and the impermeable approximations to sand, respectively, with velocity vectors in Figures 14.

Figures 15 through 20 outline the final velocity profiles for the floor emplacement configuration with the drift filled with clay. The horizontal and vertical velocities at discrete points along a path from below the drift to the top of the mesh are plotted in Figures 15 and 16. In Figures 17 and 18 the path has been moved to the right approximately half the width of the drift so that it is through tuff only. Figures 19 and 20 show the two components of velocity from the left-hand boundary to the right, midway up the height of the drift. The horizontal velocities in the tuff along the top of the drift increase toward the right, as some water is diverted to flow around the drift. Under the drift the horizontal velocities reverse direction and then decrease in magnitude as the water turns to spread out in the tuff below. However, the horizontal velocities along each of the three paths are an order of magnitude smaller than the influx rate. The vertical velocities are affected in a relatively narrow band beginning within 3 m of the top. Below the drift the velocities are affected by the impermeable zone; they increase slightly, near the waste package, because there is less volume in which the water can travel. The downward velocities decrease inside the drift.

Figures 21 through 26 show the components of velocity in the vicinity of an impermeable drift. Again the horizontal and vertical velocities of discrete points are plotted along paths from below the drift to the top of the mesh, parallel and to the right of the first path, and from the left-hand to the right-hand boundaries. The plots illustrate the same qualitative flow around the drift as seen in the clay-filled drift. However, since no flow is allowed inside the drift, the horizontal flow is larger with an impermeable drift, and the vertical velocity through the drift goes to zero. The direction (sign) of the horizontal velocity changes as the groundwater flows around the drift at the top and then flows back under the drift. The vertical flow to the side of the impermeable drift is higher than the flow near a clay-filled drift, again because no water is allowed through the drift.

Modified Permeability



Impermeable

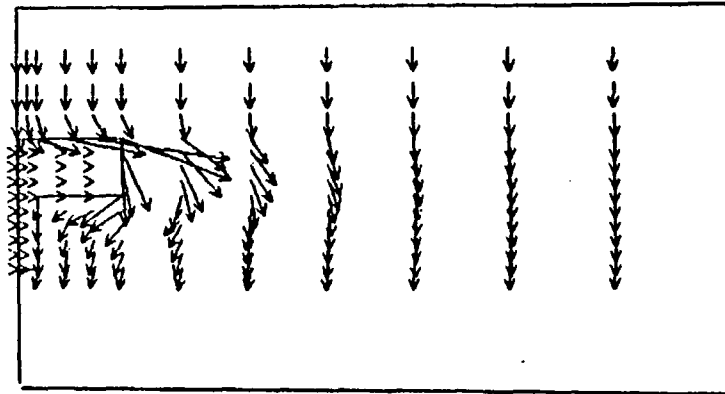
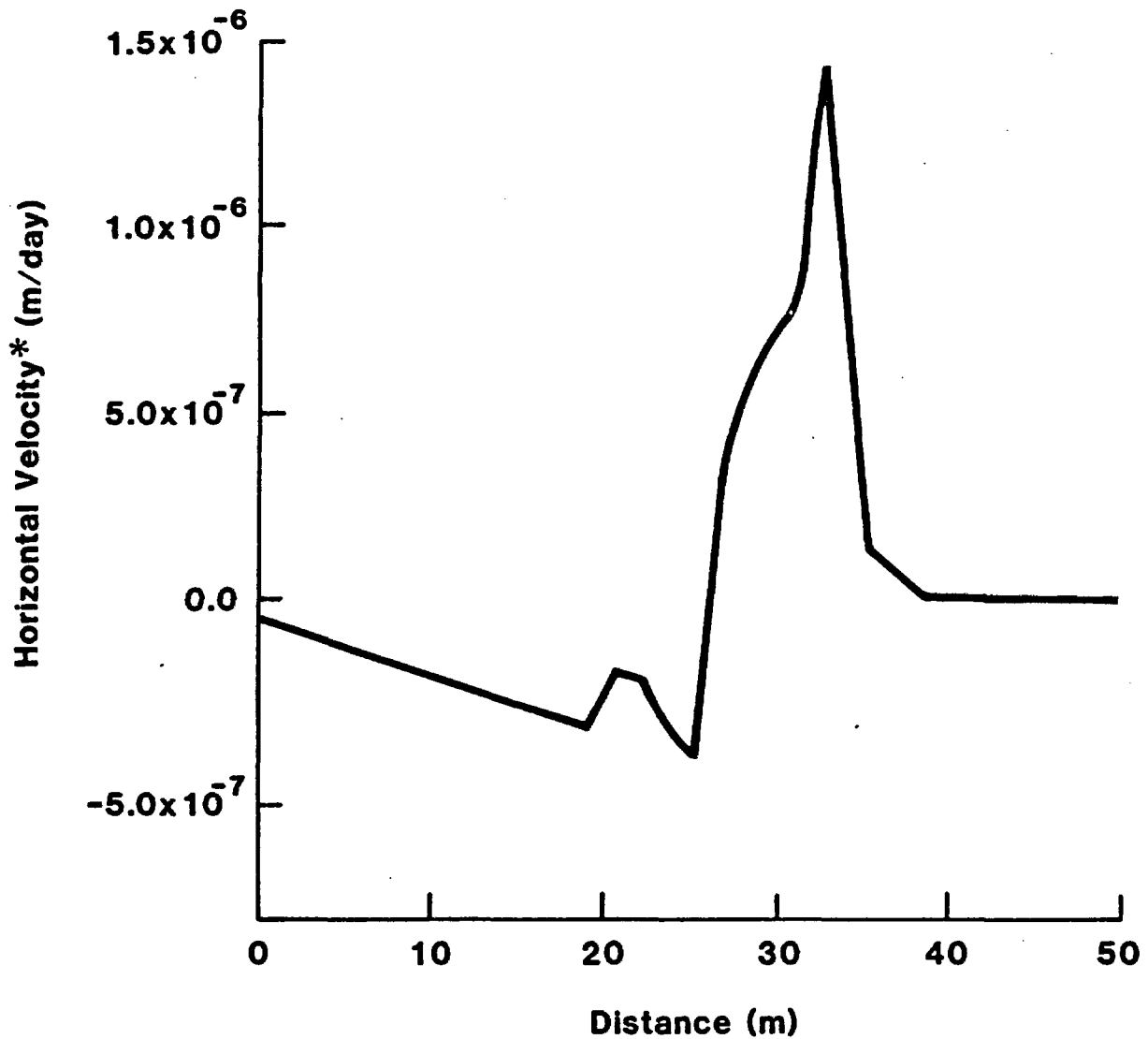
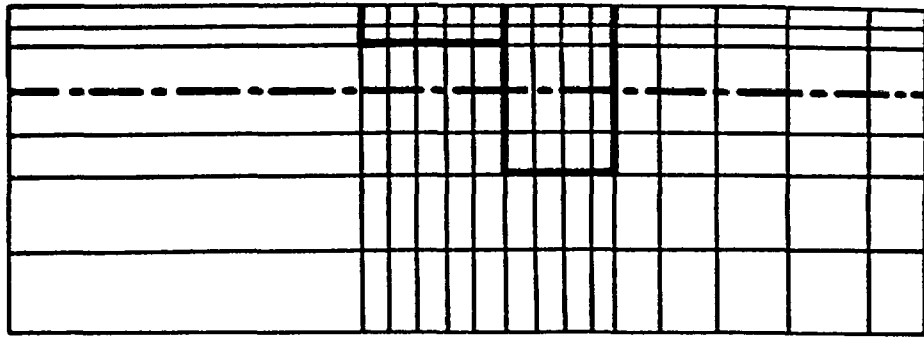
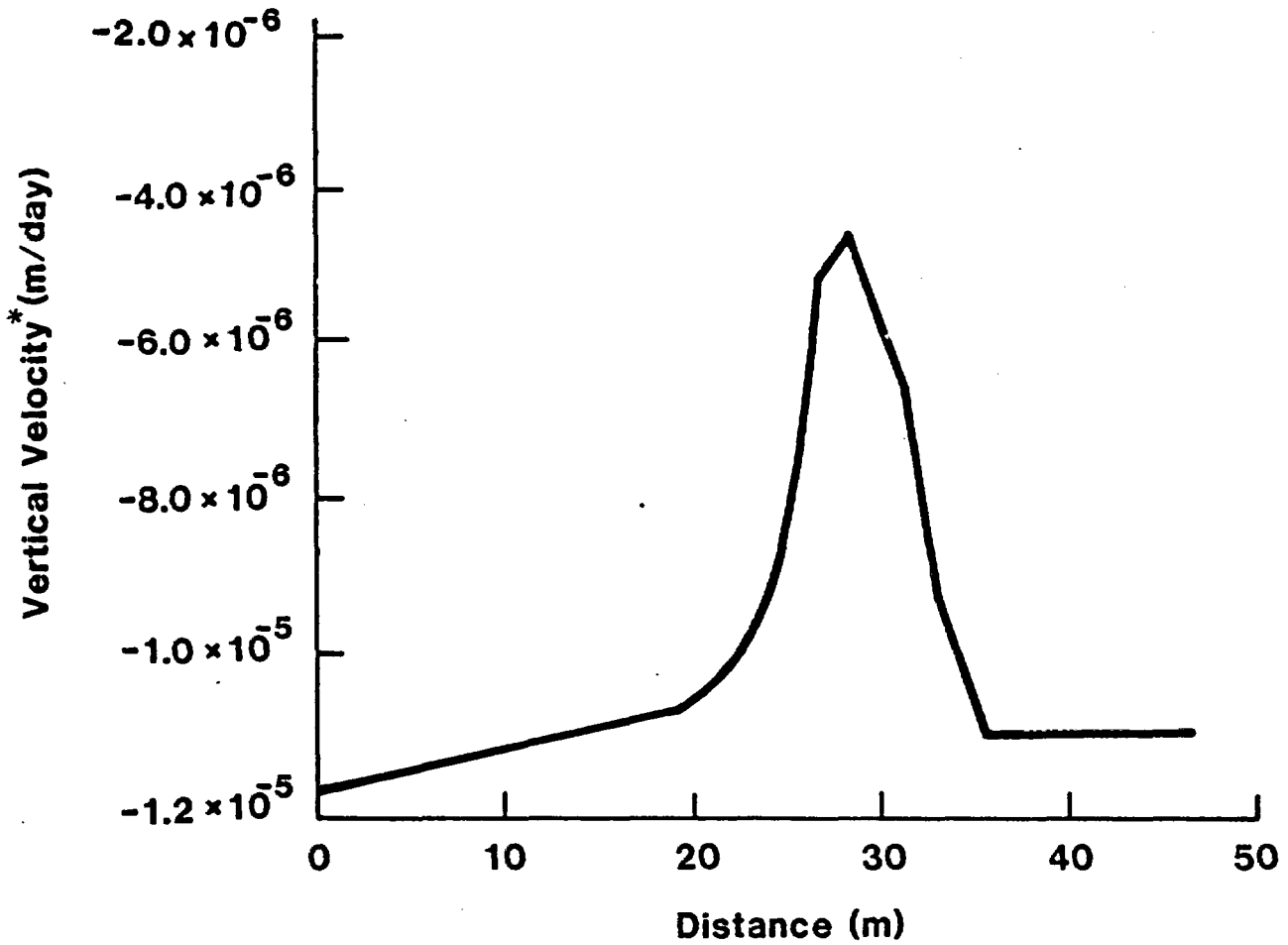
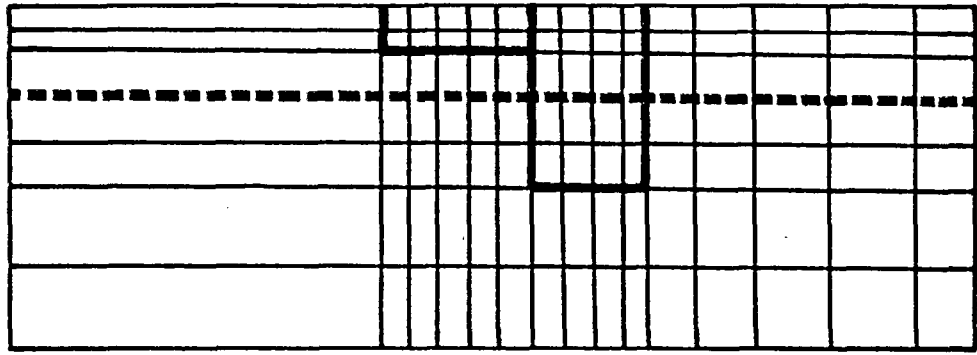


Figure 14. Velocity vectors of steady-state flow near a sand-filled drift (sand modeled with modified permeability and as an impermeable material).



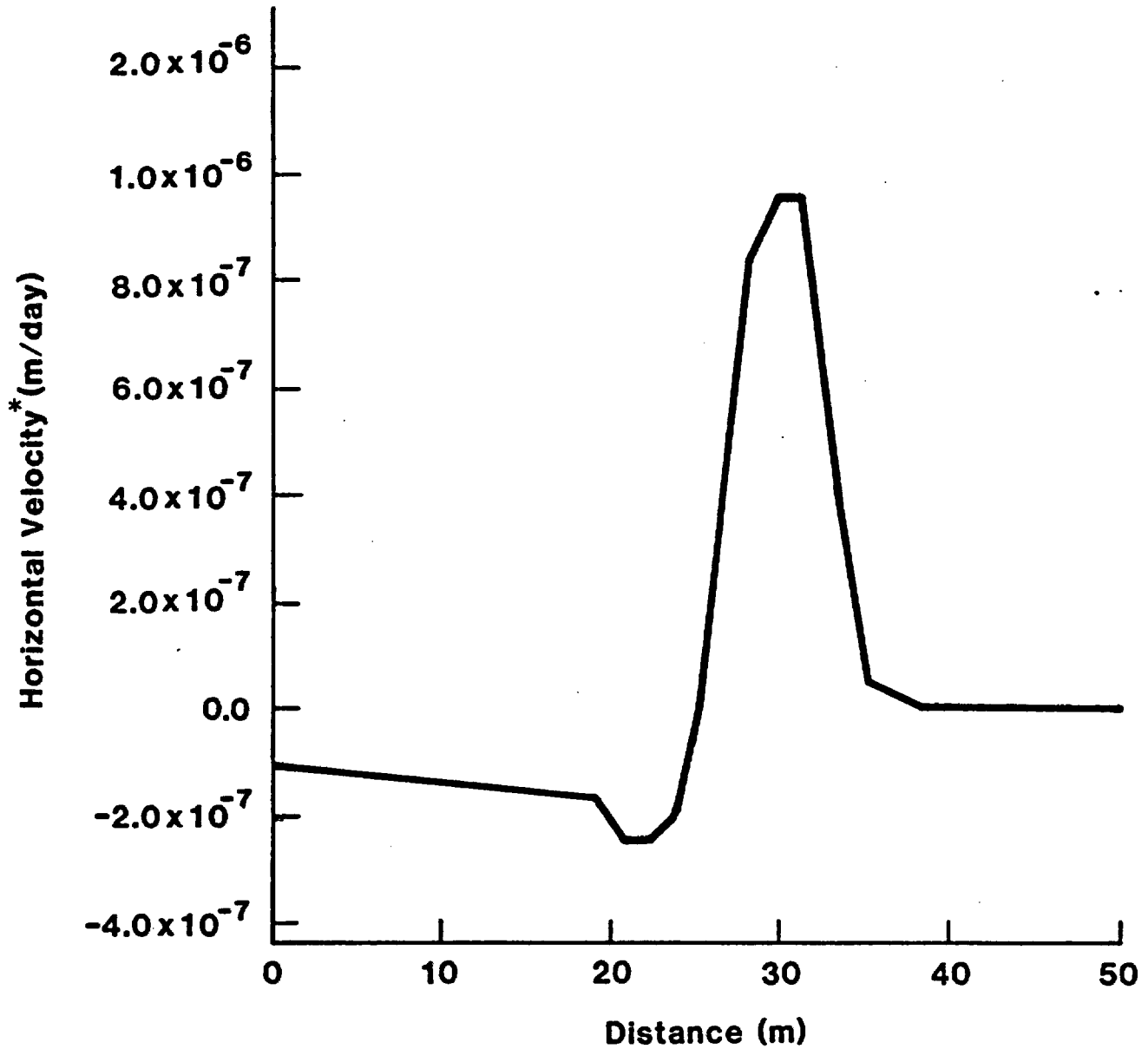
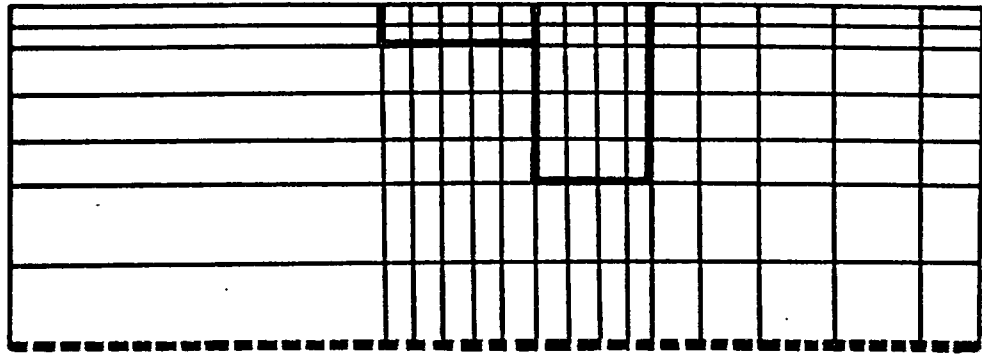
* Negative Velocities are toward the drift center line
 Positive Velocities are away from the drift center line

Figure 15. Steady-state profile of the horizontal components of velocities along a path (shown with the dotted line on the element grid above) from below the waste package through a clay-filled drift to the top boundary.



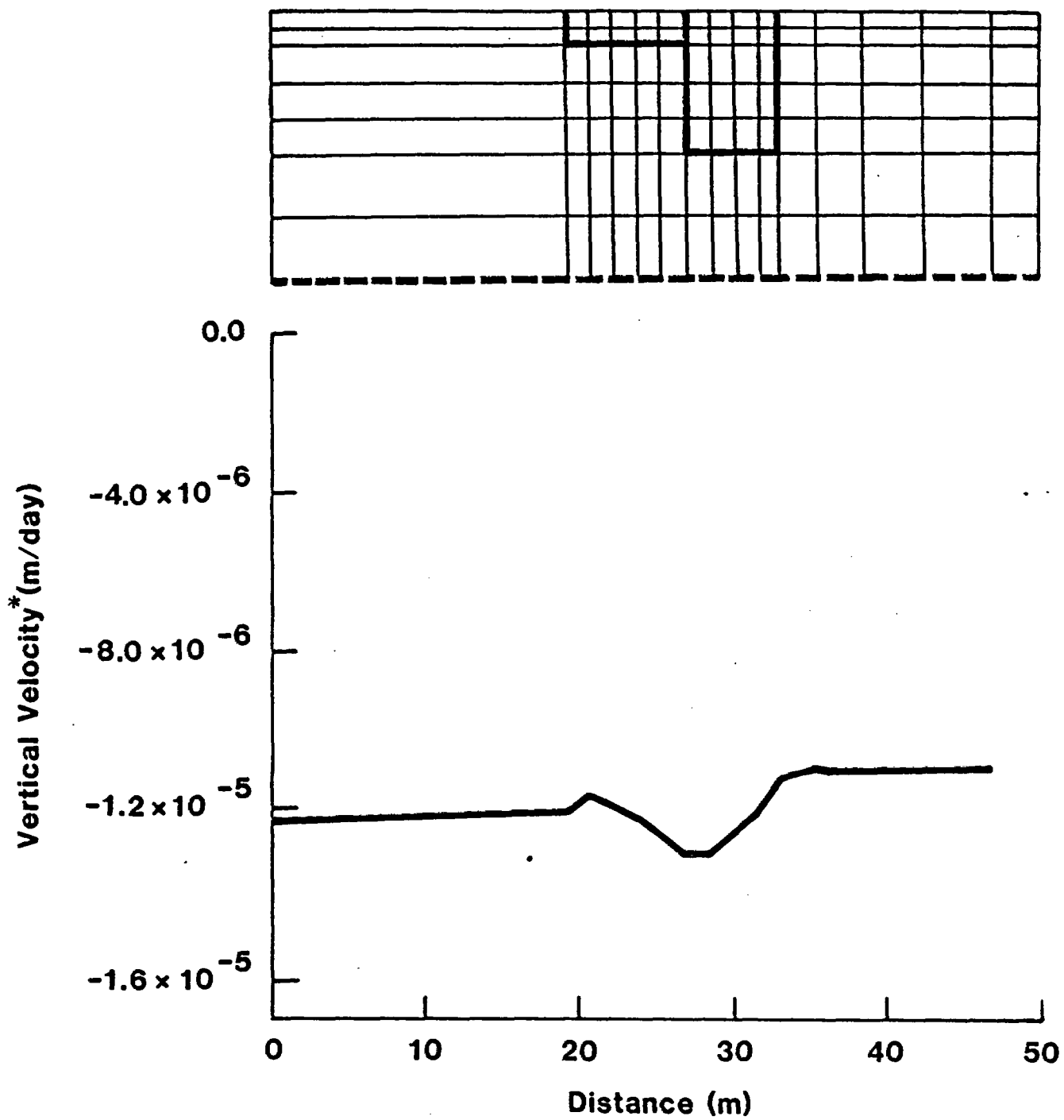
* Negative Velocities are downward

Figure 16. Steady-state profile of the vertical components of velocities along a path (shown with the dotted line on the element grid above) from below the waste package through a clay-filled drift to the top boundary.



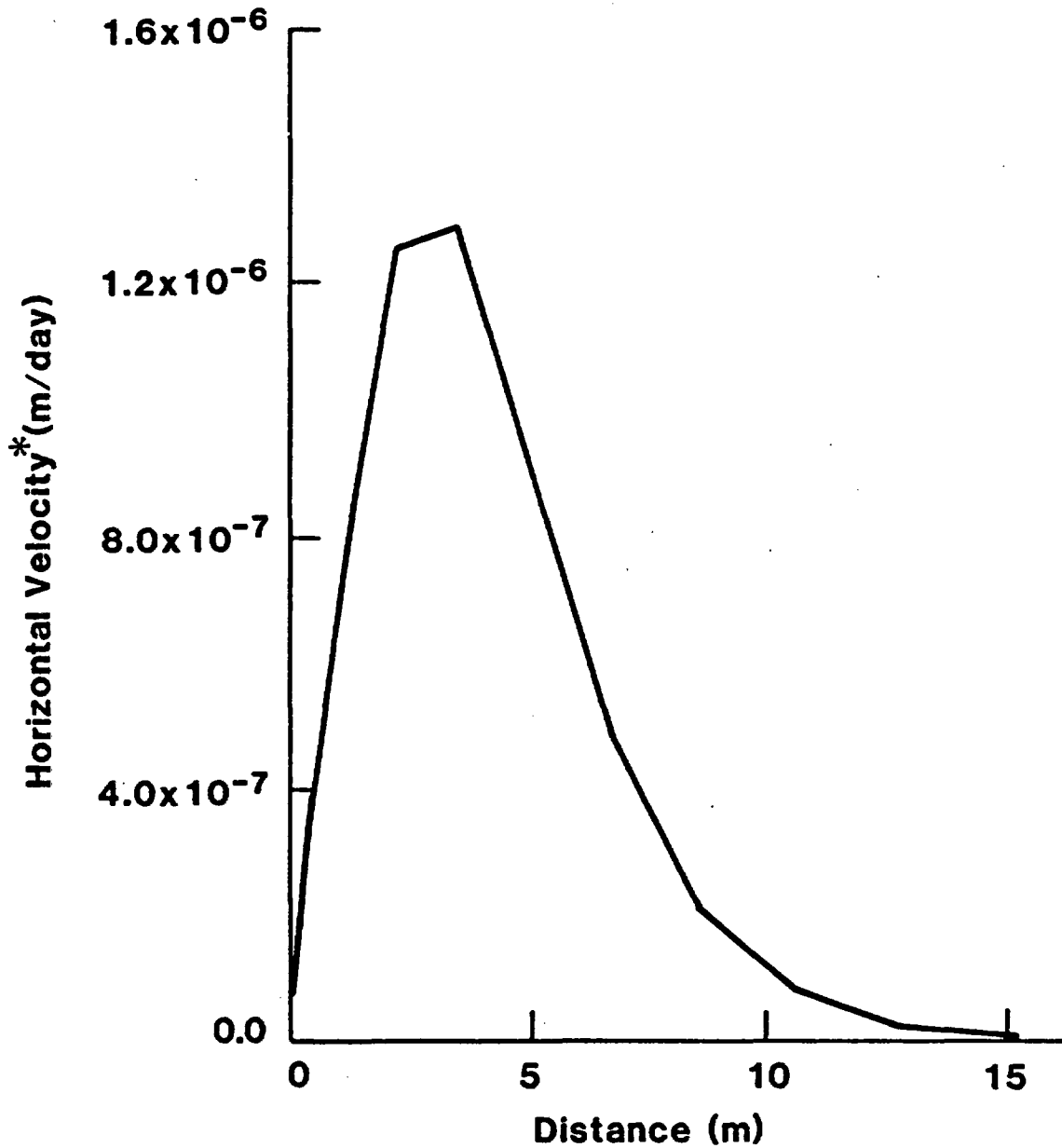
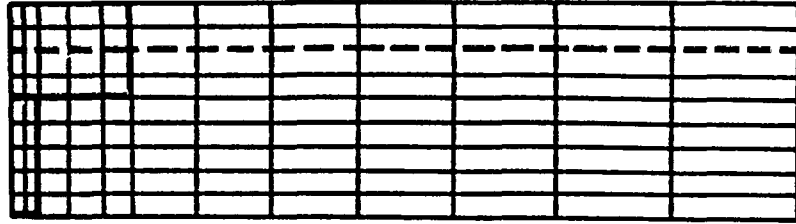
* Negative Velocities are toward the drift centerline
 Positive Velocities are away from the drift centerline

Figure 17. Steady-state profile of the horizontal components of velocities along a path (shown with the dotted line on the element grid above) approximately 2.3 m to the side of a clay-filled drift.



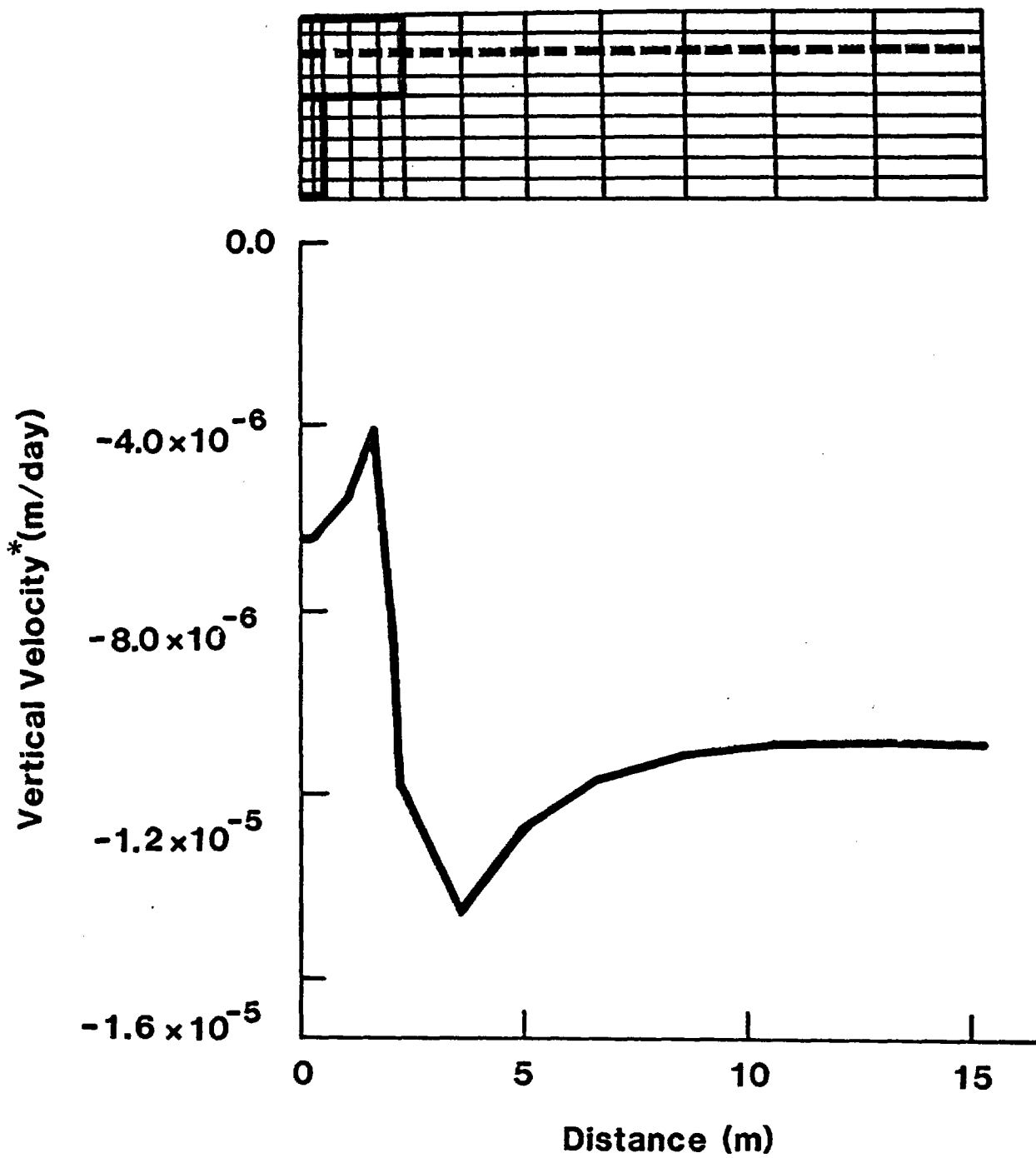
* Negative Velocities are downward

Figure 18. Steady-state profile of the vertical components of velocities along a path (shown with the dotted line on the element grid above) approximately 2.3 m to the side of a clay-filled drift.



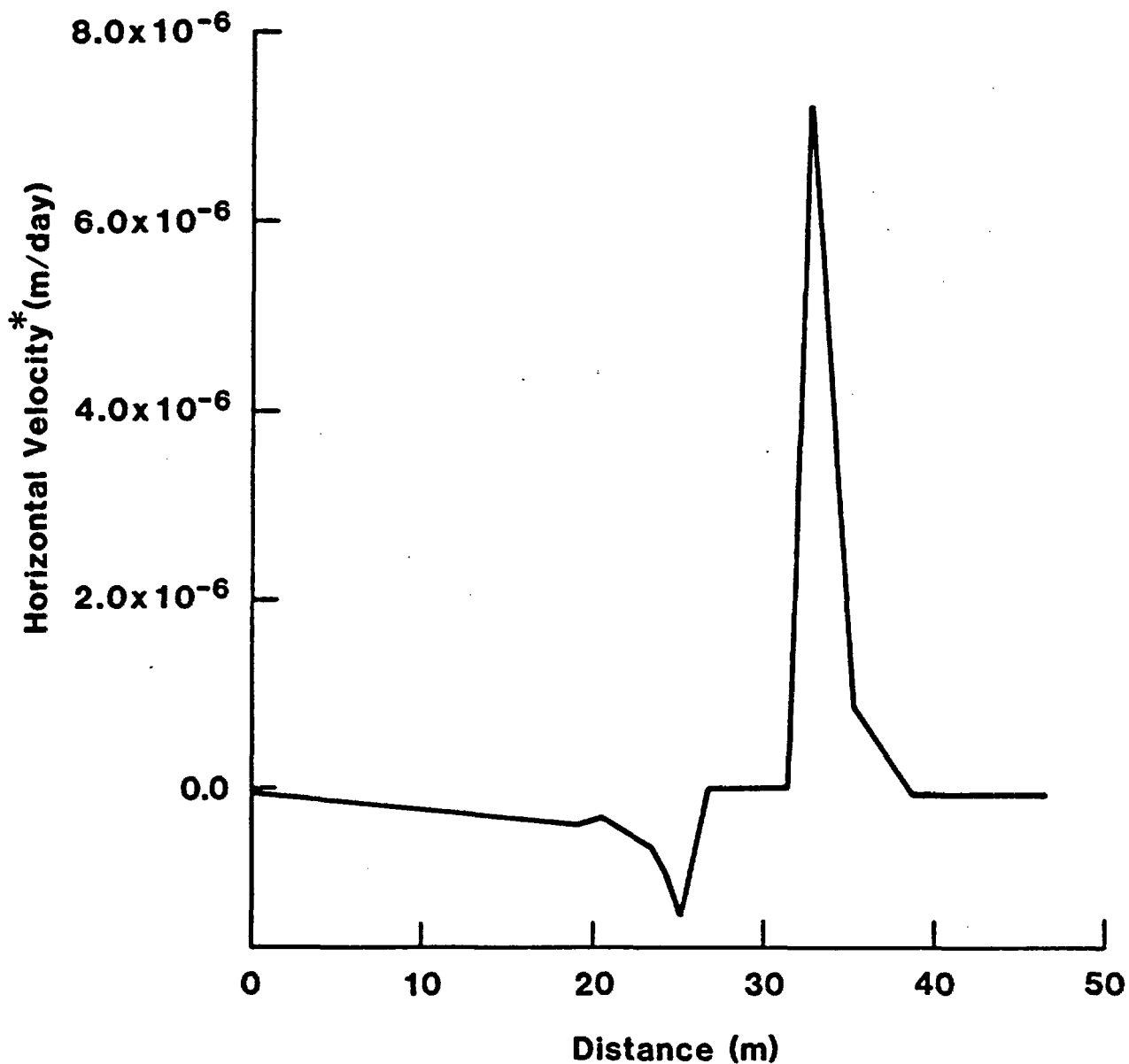
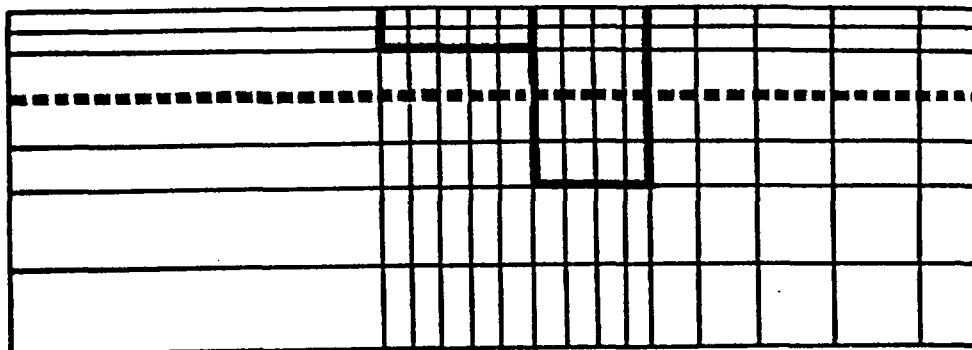
* Positive Velocities are away from the drift center line

Figure 19. Steady-state profile of the horizontal components of velocities along a path (shown with the dotted line on the element grid above) through a clay-filled drift from the left to the right side boundary.



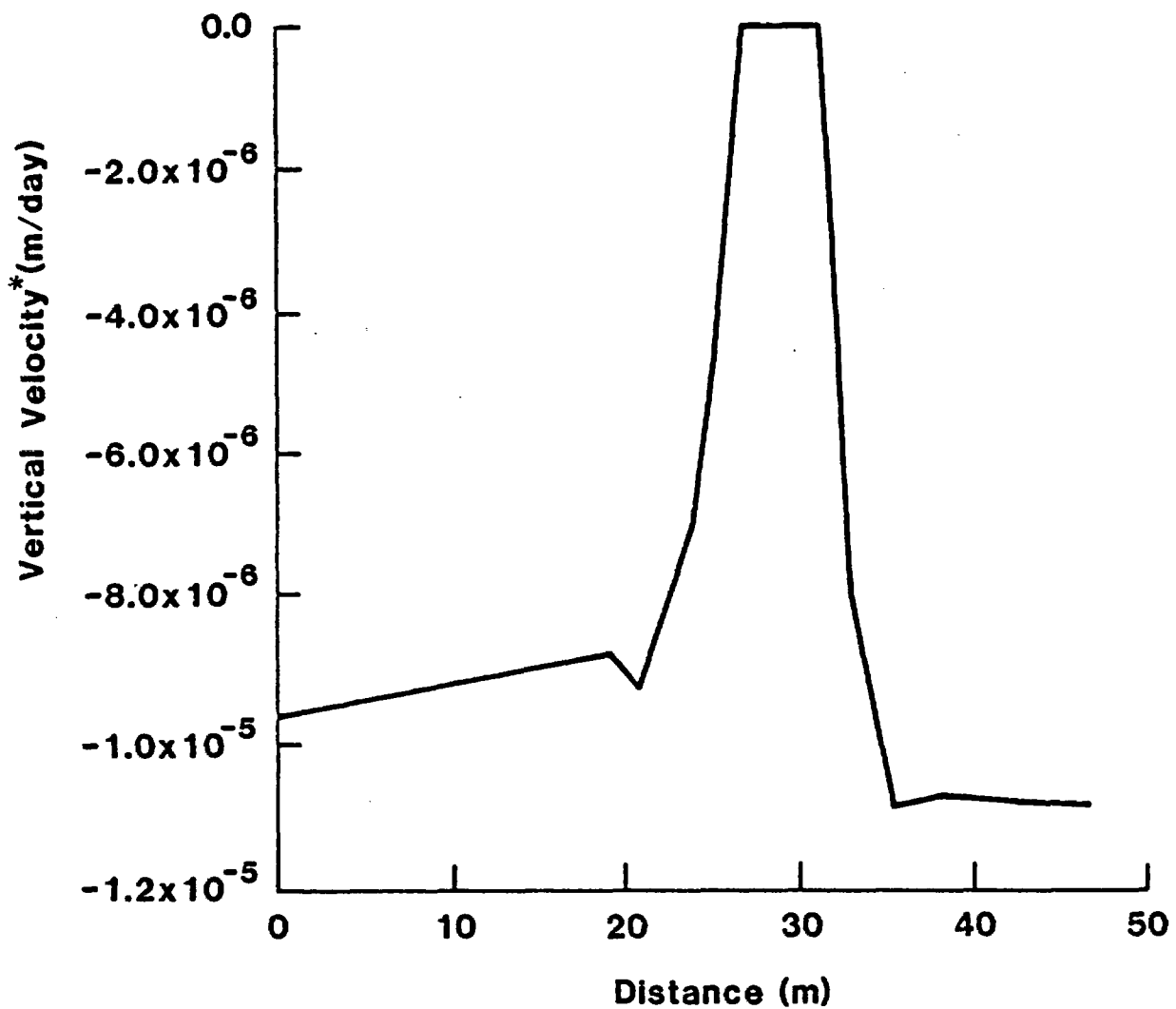
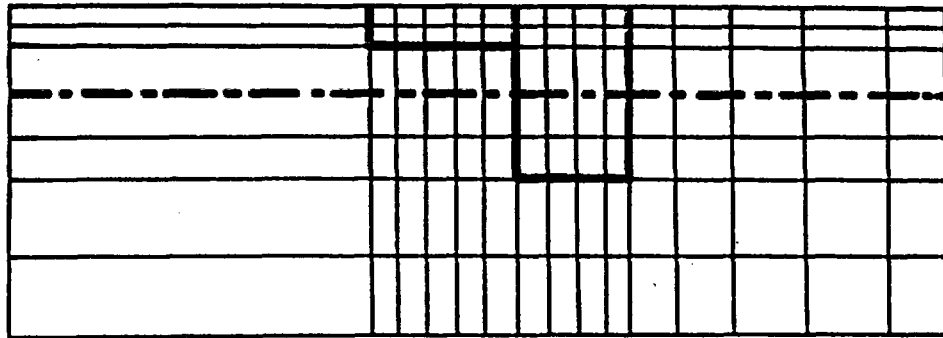
*Negative Velocities are downward

Figure 20. Steady-state profile of the vertical components of velocities along a path (shown with the dotted line on the element grid above) through a clay-filled drift from the left to the right side boundary.



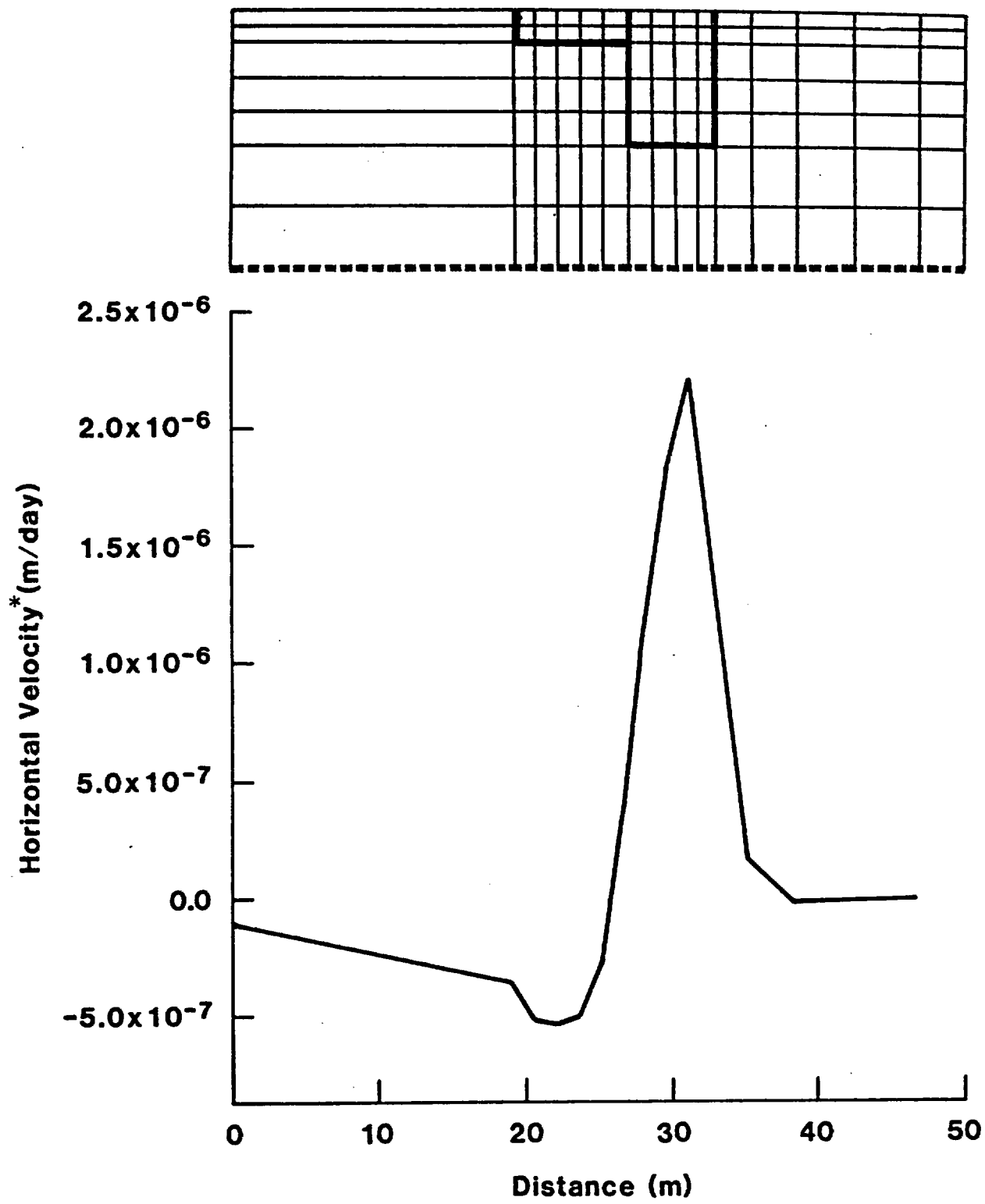
* Negative Velocities are toward the drift center line
 Positive Velocities are away from the drift center line

Figure 21. Steady-state profile of the horizontal components of velocities along a path (shown with the dotted line on the element grid above) from below the waste package through an impermeable drift to the top boundary.



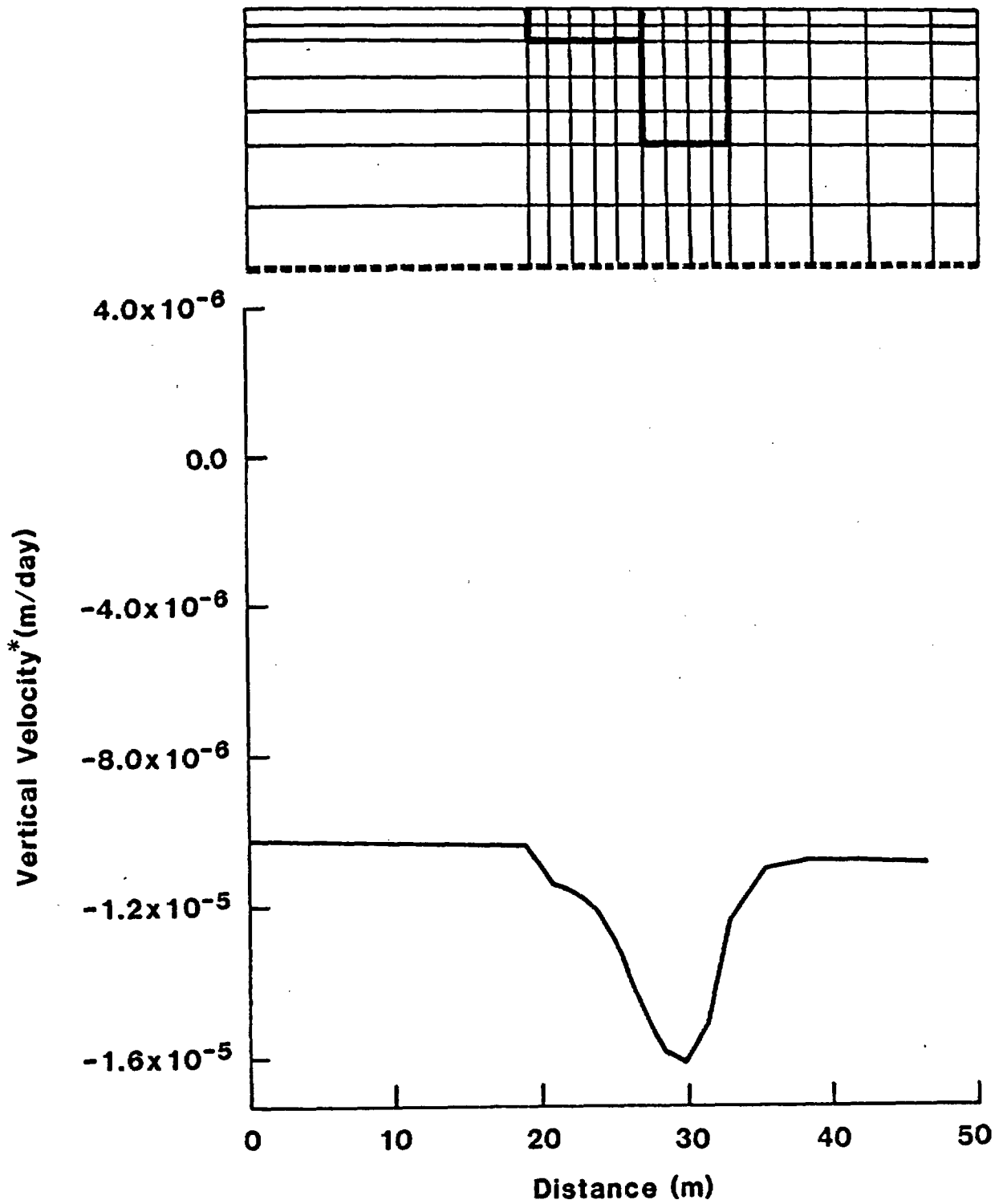
*Negative Velocities are downward

Figure 22. Steady-state profile of the vertical components of velocities along a path (shown with the dotted line on the element grid above) from below the waste package through an impermeable drift to the top boundary.



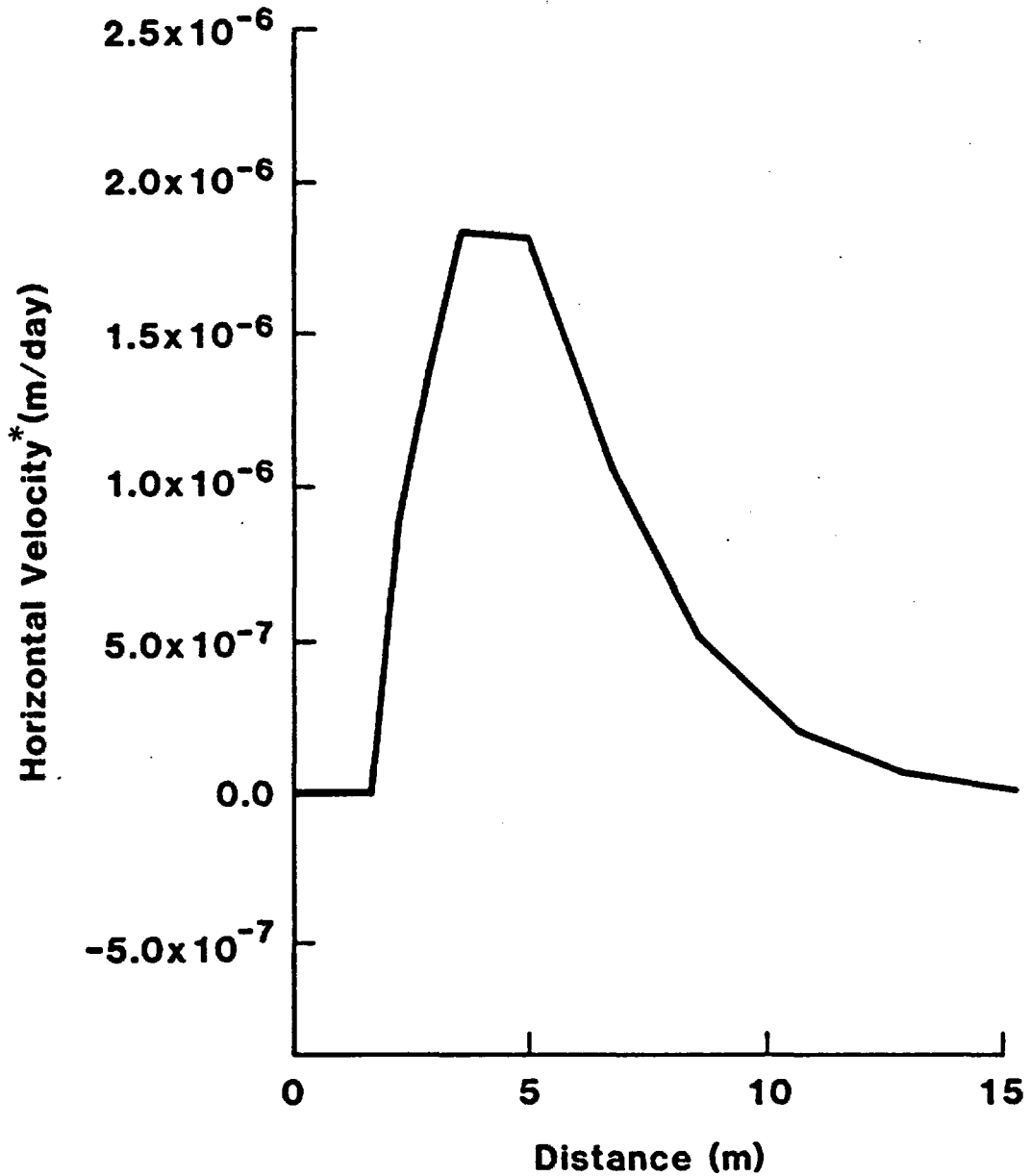
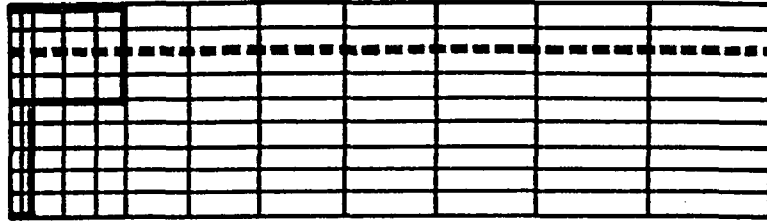
* Negative Velocities toward the drift centerline
 Positive Velocities are away from the drift center line

Figure 23. Steady-state profile of the horizontal components of velocities along a path (shown with the dotted line on the element grid above) approximately 2.3 m to the side of an impermeable drift.



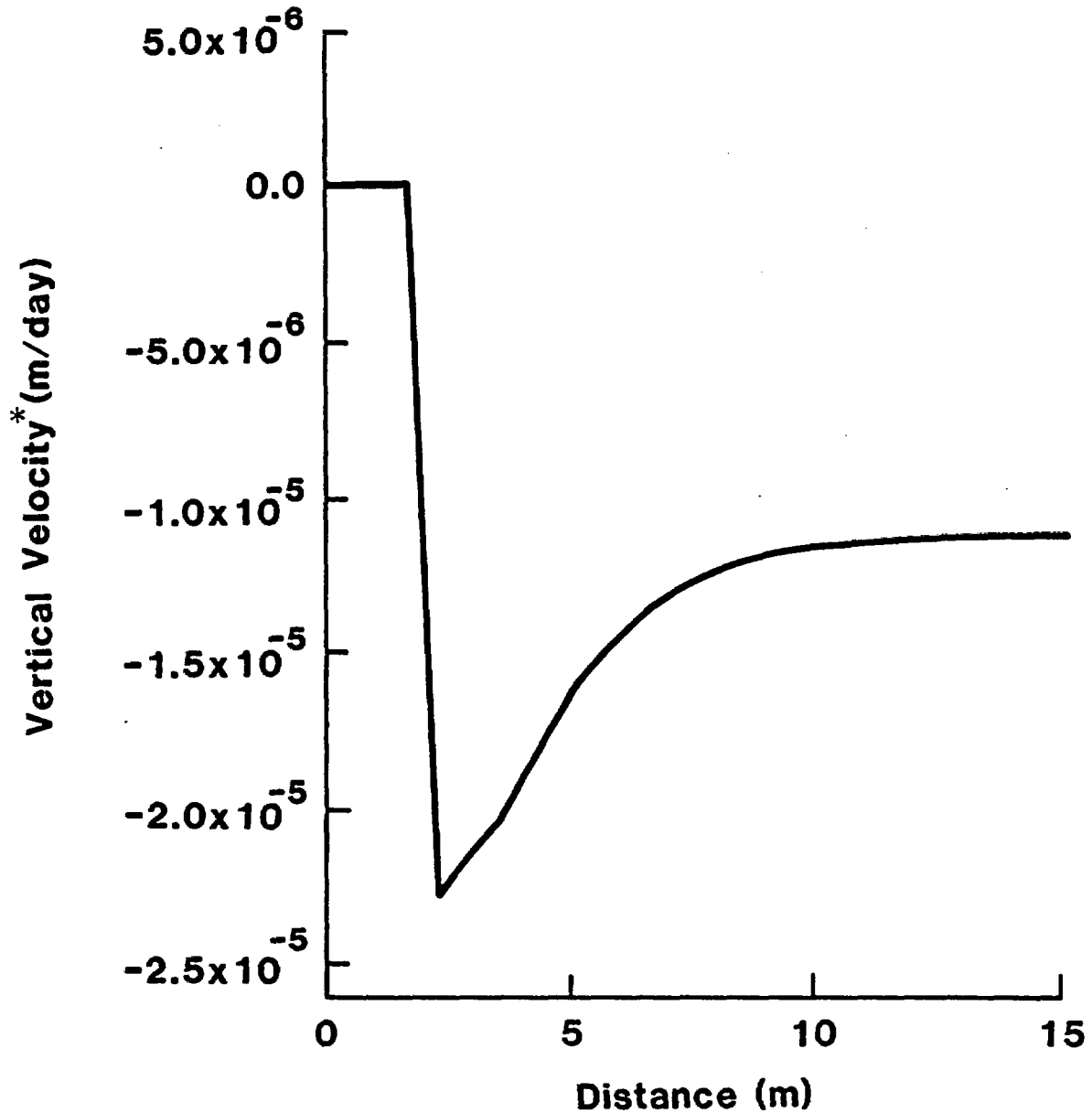
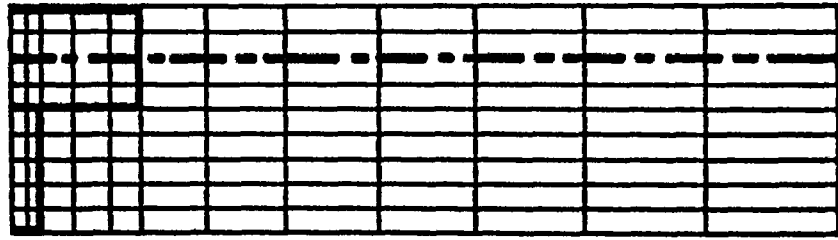
* Negative Velocities are downward

Figure 24. Steady-state profile of the vertical components of velocities along a path (shown with the dotted line on the element grid above) approximately 2.3 m to the side of an impermeable drift.



***Positive Velocities are away from the drift centerline**

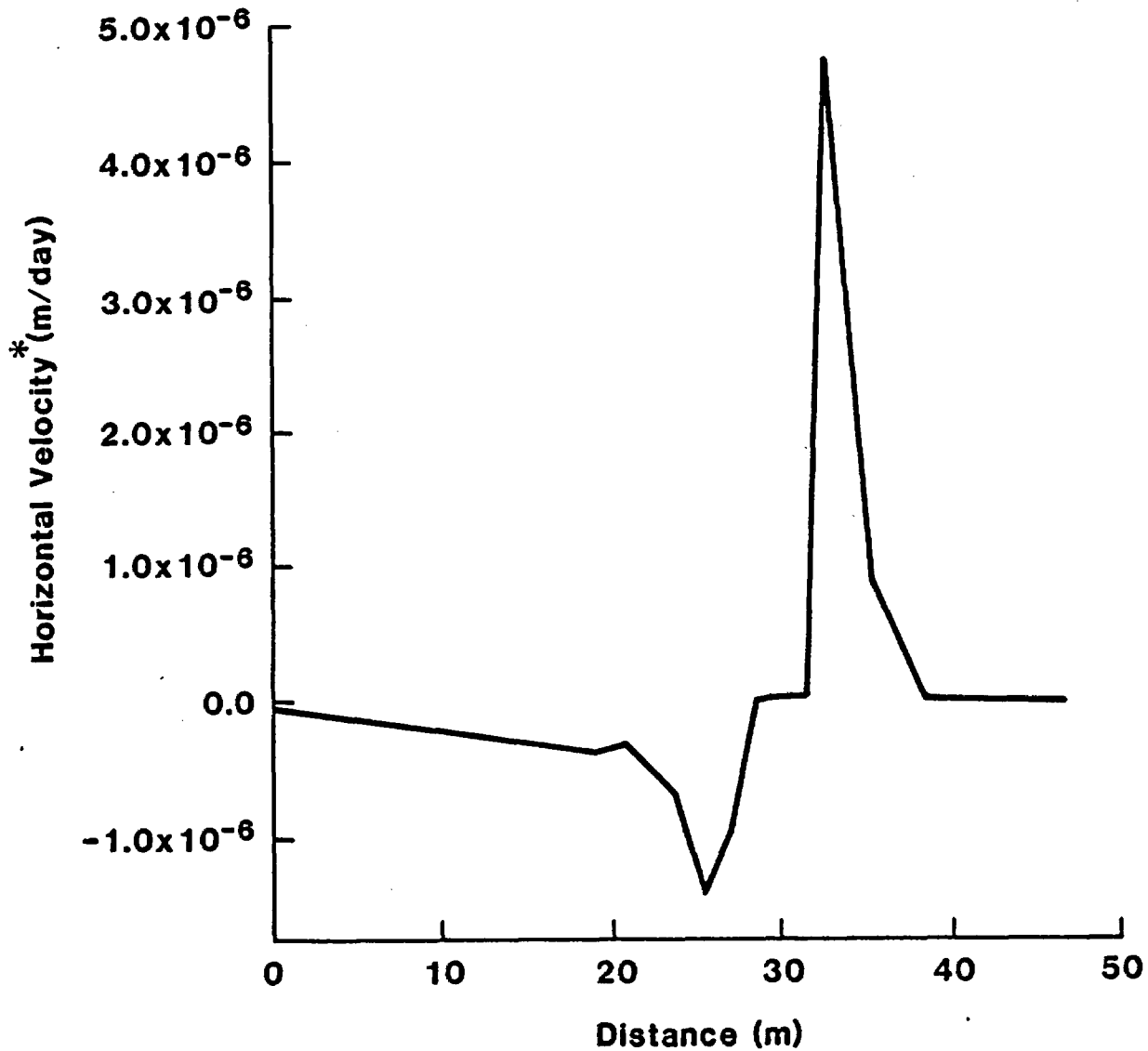
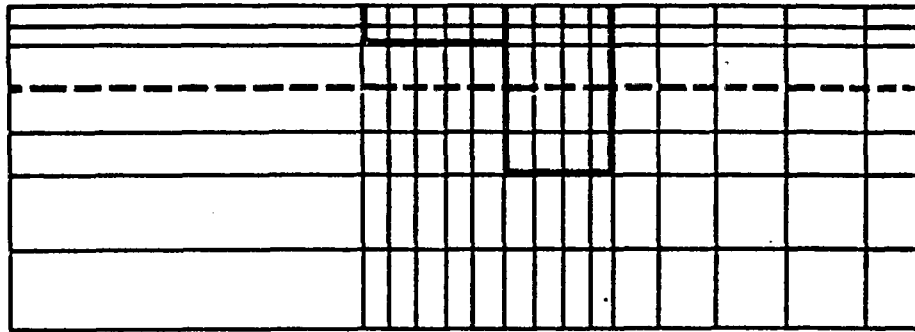
Figure 25. Steady-state profile of the horizontal components of velocities along a path (shown with the dotted line on the element grid above) through an impermeable drift from the left to the right side boundary.



* Negative Velocities are downward

Figure 26. Steady-state profile of the vertical components of velocities along a path (shown with the dotted line on the element grid above) through an impermeable drift from the left to the right side boundary.

Figures 27 through 32 are velocity profile plots for a drift filled with sand (having the modified permeability characteristic curve). The qualitative behavior is the same as that calculated when the drift is assumed impermeable. The horizontal velocities in Figures 27 and 29 are slightly smaller than those seen in Figures 21 and 23 because some of the water is allowed to flow through the drift. For the same reason, the vertical velocities in Figures 28 and 32 do not go exactly to zero in the drift. Recall that all of the velocities have about a 12% error band associated with them, as discussed in Section 4 of this report.



* Negative Velocities are toward the drift center line
 Positive Velocities are away from the drift center line

Figure 27. Steady-state profile of the horizontal components of velocities along a path (shown with the dotted line on the element grid above) from below the waste package through a (modified permeability) sand-filled drift to the top boundary.

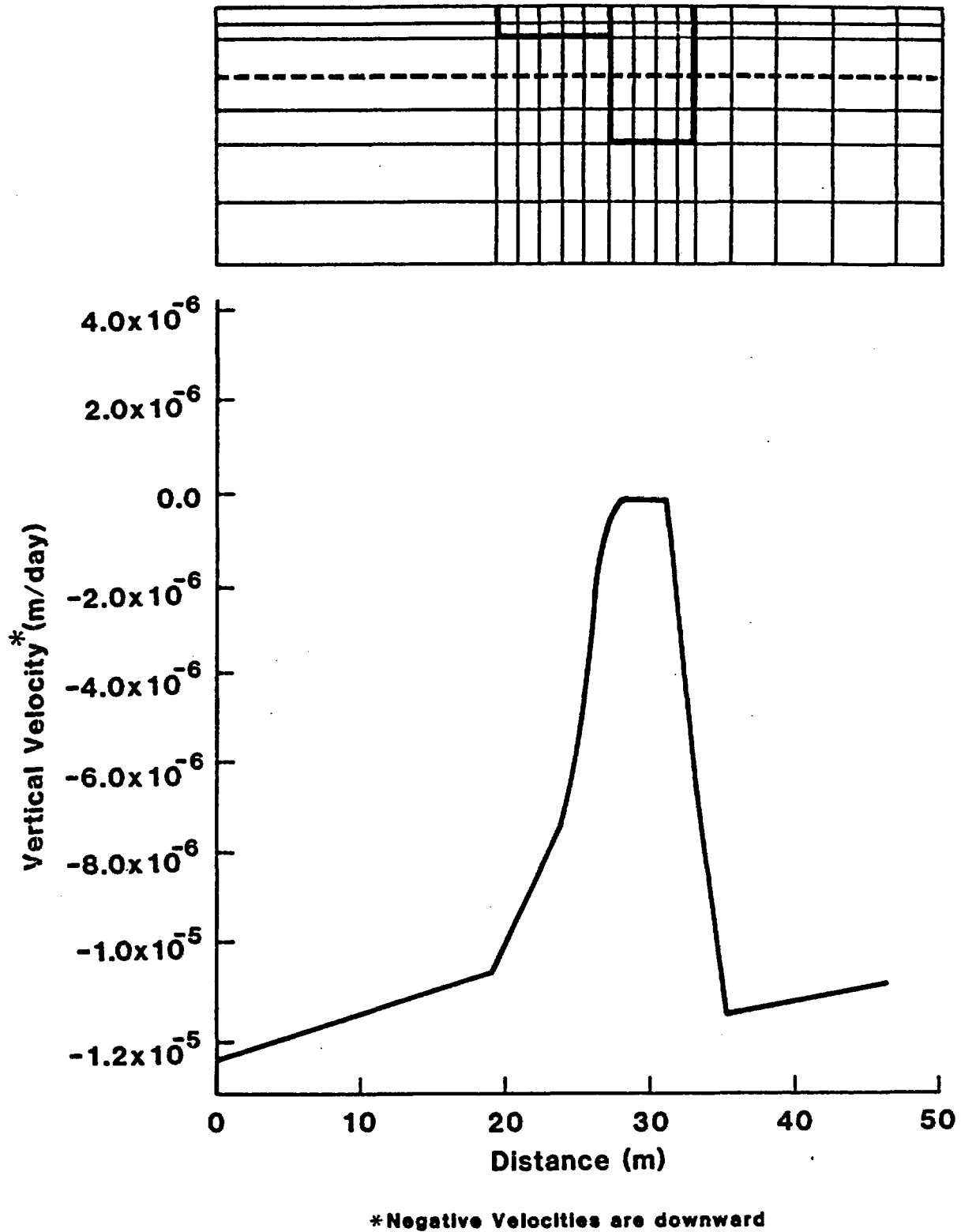
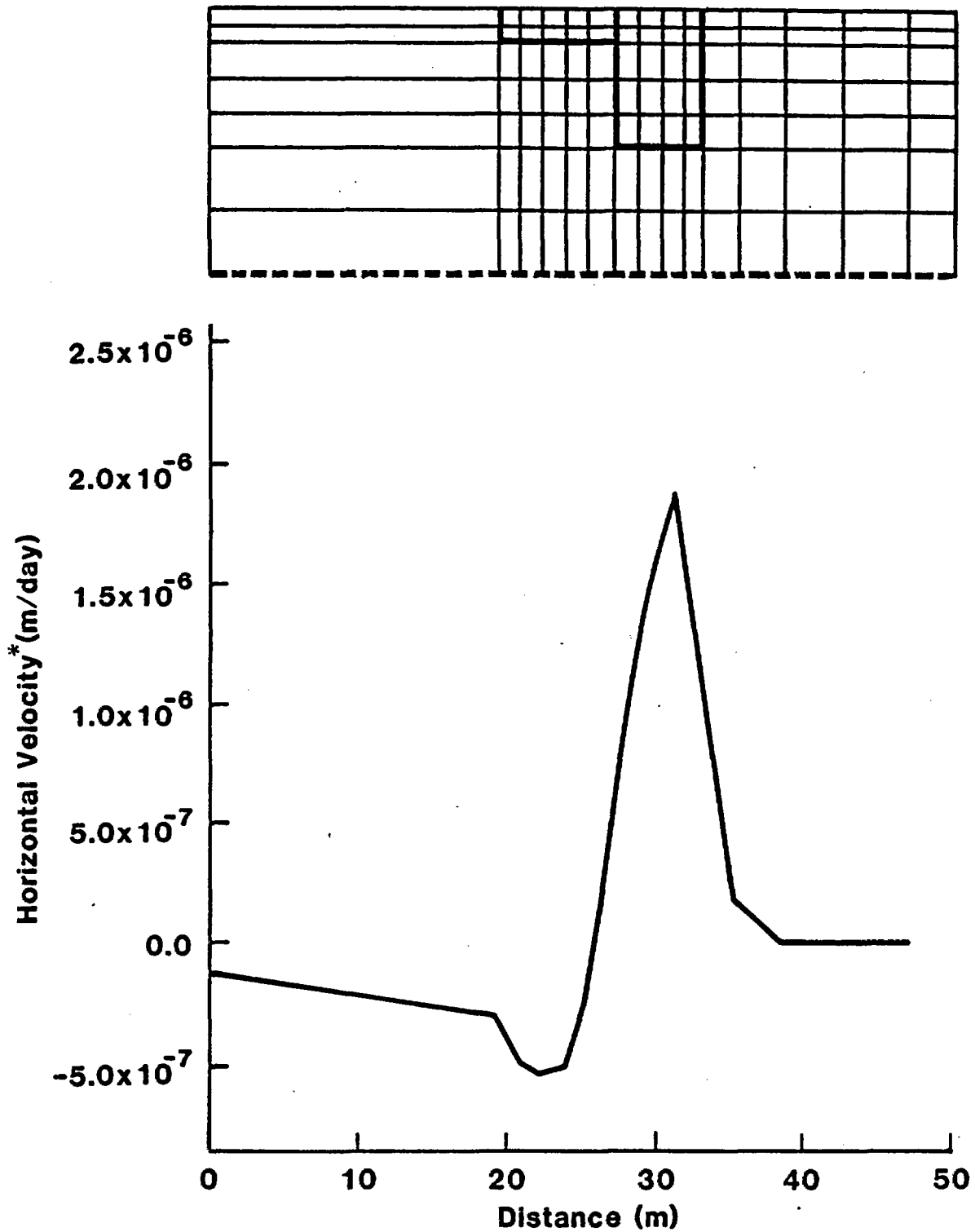
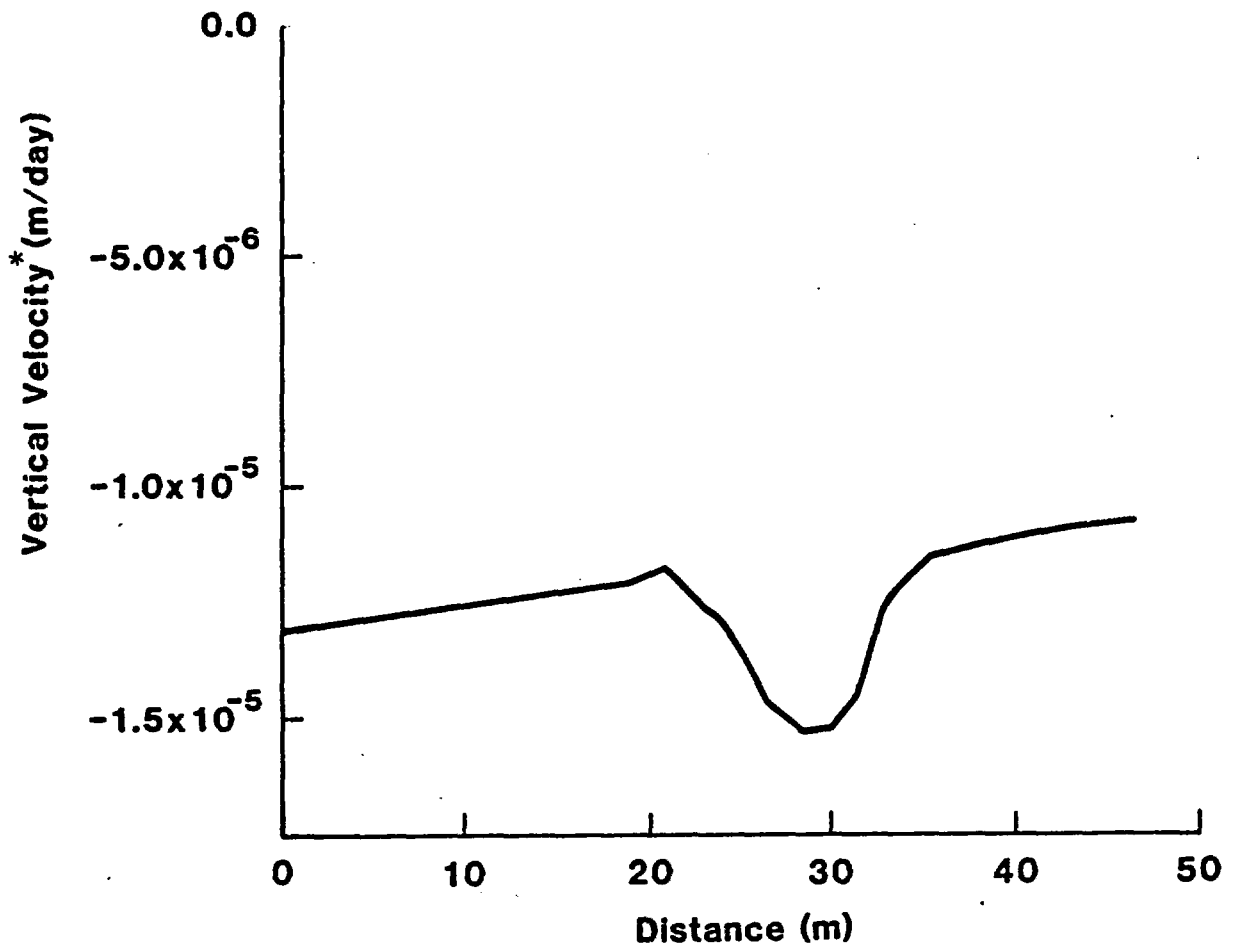
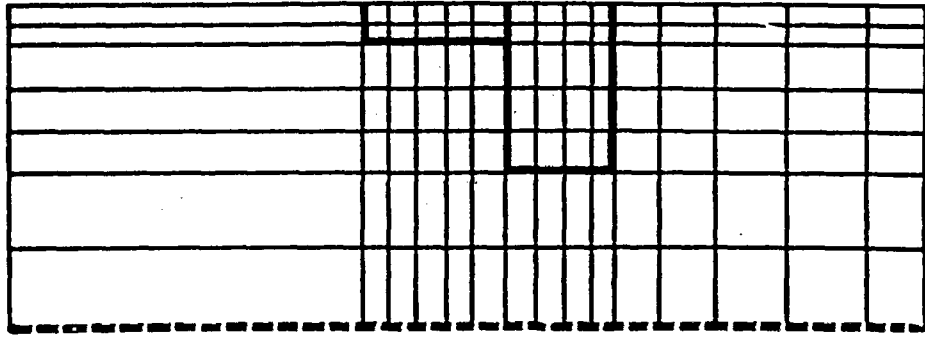


Figure 28. Steady-state profile of the vertical components of velocities along a path (shown with the dotted line on the element grid above) from below the waste package through a (modified permeability) sand-filled drift to the top boundary.



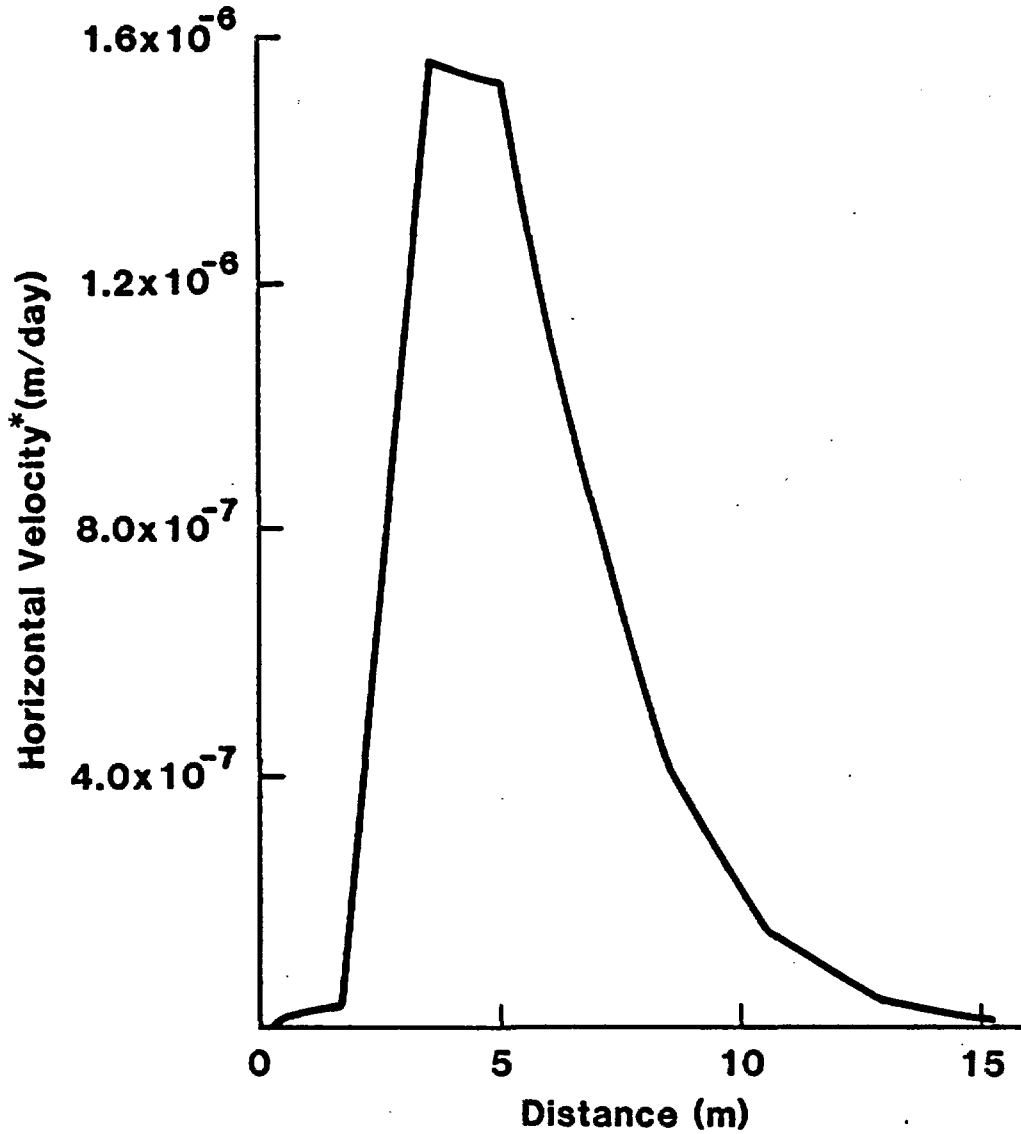
* Negative Velocities are toward the drift centerline
 Positive Velocities are away from the drift centerline

Figure 29. Steady-state profile of the horizontal components of velocities along a path (shown with the dotted line on the element grid above) approximately 2.3 m to the side of a (modified permeability) sand-filled drift.



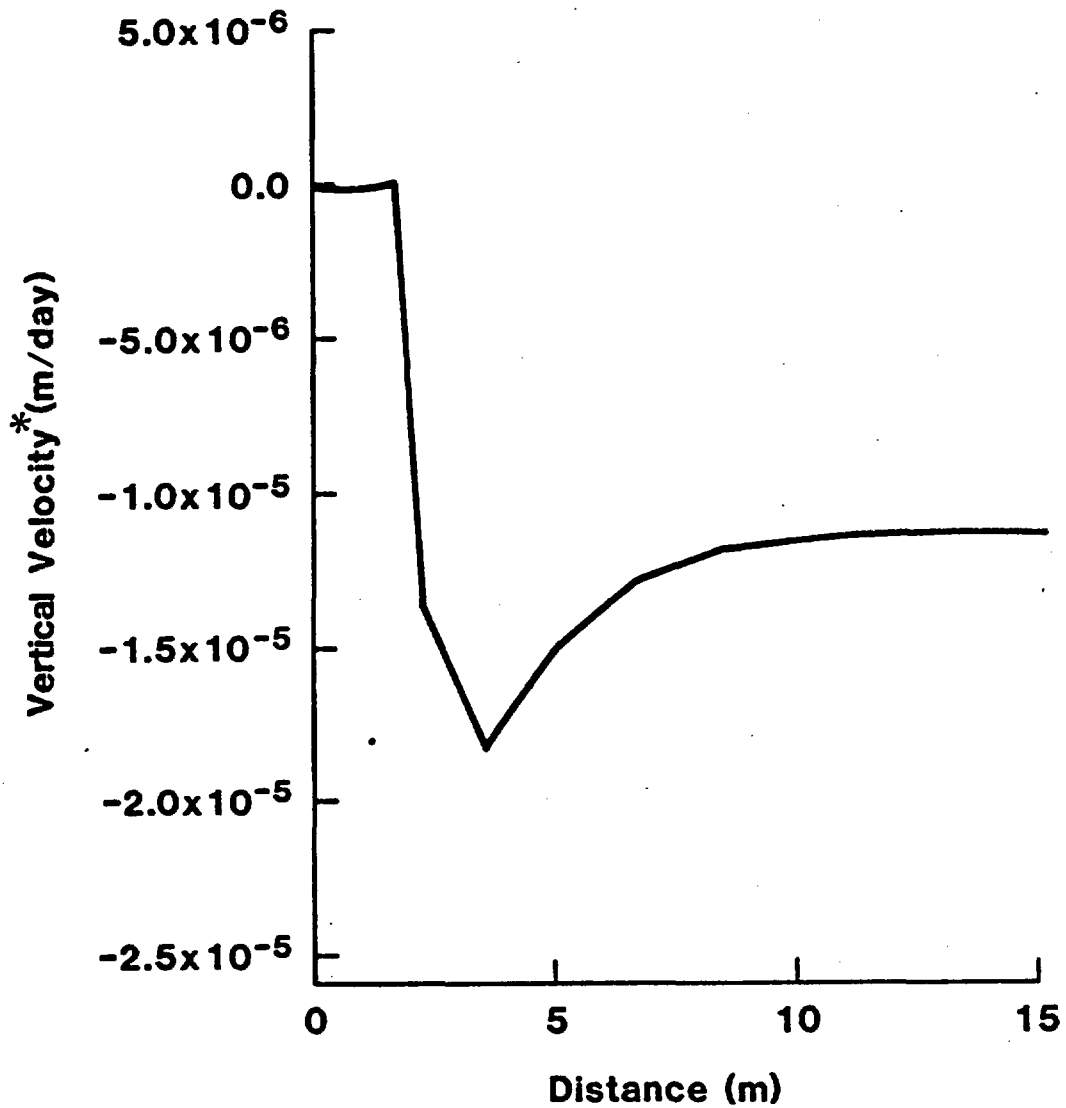
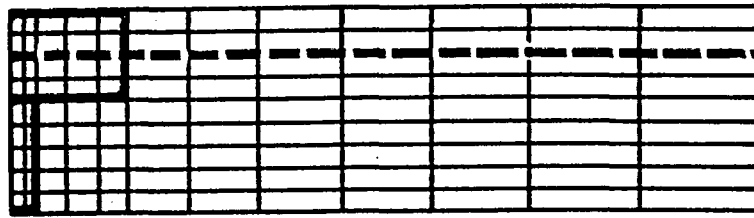
* Negative Velocities are downward

Figure 30. Steady-state profile of the vertical components of velocities along a path (shown with the dotted line on the element grid above) approximately 2.3 m to the side of a (modified permeability) sand-filled drift.



* Positive Velocities are away from the drift centerline

Figure 31. Steady-state profile of the horizontal components of velocities along a path (shown with the dotted line on the element grid above) through a (modified permeability) sand-filled drift from the left to the right side boundary.



*Negative Velocities are downward

Figure 32. Steady-state profile of the vertical components of velocities along a path (shown with the dotted line on the element grid above) through a (modified permeability) sand-filled drift from the left to the right side boundary.

6. SUMMARY AND CONCLUSIONS

In this analysis, we calculate the flow past the waste package below a clay-filled drift to be over 91% of the influx rate. The velocities near the waste package below a sand-filled drift are over 81% of the influx. This indicates that backfilling the drift with sand or clay does lower the flow past the waste package from the undisturbed influx; however, it appears that backfilling a drift with clay does not provide significant reduction of flow in the vicinity of the waste package in the floor emplacement configuration. Backfilling with sand instead of clay can only lower the flow another 10%.

Water is deviated only one to two drift widths to the side of the drift, even if no flow is allowed through the drift. Although, in this model, the side boundary conditions are lines of symmetry for a floor emplacement configuration, conclusions can be drawn regarding a wall emplacement configuration in which waste packages are placed horizontally in boreholes between the drifts. The fact that the groundwater does not flow a significant distance to the side of the drift implies that the drift would not influence flow past a waste package in the wall emplacement design if a stand-off distance between the drift and the waste is included in the design.

Because of the extremely large gradients in permeability with pressure for sand, numerical difficulties occurred in modeling a sand-filled drift in unsaturated tuff. The behavior of the sand as a backfill had to be approximated. Two approximations were considered: the permeability versus pressure characteristic curve was modified to be less steep, and the sand was modeled as a completely impermeable material. The two approximations yielded very similar velocities (differing by 2% or less) immediately adjacent to the waste package.

There are several limitations to this analysis. The model is two-dimensional, which creates an artificially high influence of the assumed impermeable waste package below the drift. Obviously, the magnitude of the calculated steady-state velocities are dependent on the assumed influx; however, because the boundary conditions and the characteristic curves determine the steady-state pressure profiles, not only the velocities, but

also the final saturations are dependent on the assumed hydrologic properties and influx rate. Probably the most influential approximation is that the flow is modeled as matrix flow, ignoring possible fractures.

ACKNOWLEDGMENTS

The authors would like to thank Mario Martinez for his comments and review of this report. Acknowledgement should also go to Joe Fernandez who helped define the problem, provided many of the needed parameters, and reviewed the report.

REFERENCES

1. Eaton, R. R., Gartling, D. K., and Larsen, D. E., "SAGUARO -- A Finite Element Computer Program for Partially Saturated Porous Flow Problems," Sandia National Laboratories, Report No. SAND82-2772 (1983).
2. Freeze, R. A. and Cherry, J. A., Groundwater, Prentice-Hall, Inc., 1979.
3. Mondy, L. A., Wilson, R. K., and Bixler, N. E., "Comparison of Waste Emplacement Configurations for a Nuclear Waste Repository in Tuff. IV. Thermo-Hydrological Analysis," Sandia National Laboratories, Report No. SAND83-0757 (1983).
4. Memo regarding: Numerical Calculations for the NNWSI Repository Sealing Program, from J. A. Fernandez to J. W. Nunziato and L. A. Mondy, dtd. February 7, 1983.
5. CRC Handbook of Chemistry and Physics, 54th ed., Weast, R. C., Ed., 1973-1974.
6. Mualem, Y., "A Catalog of the Hydraulic Properties of Unsaturated Soils", Hydrodynamics and Hydraulic Laboratory, Technion Israel Institute of Technology, Haifa, Israel, Research Project 442, 1976.
7. Gee, G. W., "Laboratory Report on the Unsaturated Flow Characteristics of Core Samples from the Nevada Test Site Well USW-GU3 (NTS)", Draft Letter Report Prepared for Sandia National Laboratories by Pacific Northwest Laboratory, Richland, Washington.
8. Haskell, K. H. and Jones, R. E., "Brief Instructions for Using the Sandia Mathematical Subroutine Library (Version 7.2)", Sandia National Laboratories, Report No. SAND77-1441 (1978).
9. Memo regarding: Improved Time Integration Procedure for SAGUARO, from R. R. Eaton, N. E. Bixler, and B. L. Baker to N. Hayden, dtd. June 15, 1983.

DISTRIBUTION LIST

B. C. Rusche (RW-1)
Director
Office of Civilian Radioactive
Waste Management
U.S. Department of Energy
Forrestal Building
Washington, DC 20585

J. W. Bennett (RW-22)
Office of Geologic Repositories
U.S. Department of Energy
Forrestal Building
Washington, DC 20585

Ralph Stein (RW-23)
Office of Geologic Repositories
U.S. Department of Energy
Forrestal Building
Washington, DC 20585

J. J. Fiore, (RW-22)
Program Management Division
Office of Geologic Repositories
U.S. Department of Energy
Forrestal Building
Washington, DC 20585

M. W. Frei (RW-23)
Engineering & Licensing Division
Office of Geologic Repositories
U.S. Department of Energy
Forrestal Building
Washington, DC 20585

E. S. Burton (RW-25)
Siting Division
Office of Geologic Repositories
U.S. Department of Energy
Forrestal Building
Washington, D.C. 20585

C. R. Cooley (RW-24)
Geosciences & Technology Division
Office of Geologic Repositories
U.S. Department of Energy
Forrestal Building
Washington, DC 20585

T. P. Longo (RW-25)
Program Management Division
Office of Geologic Repositories
U.S. Department of Energy
Forrestal Building
Washington, DC 20585

Cy Klingsberg (RW-24)
Geosciences and Technology Division
Office of Geologic Repositories
U. S. Department of Energy
Forrestal Building
Washington, DC 20585

B. G. Gale (RW-25)
Siting Division
Office of Geologic Repositories
U.S. Department of Energy
Forrestal Building
Washington, D.C. 20585

R. J. Blaney (RW-22)
Program Management Division
Office of Geologic Repositories
U.S. Department of Energy
Forrestal Building
Washington, DC 20585

R. W. Gale (RW-40)
Office of Policy, Integration, and
Outreach
U.S. Department of Energy
Forrestal Building
Washington, D.C. 20585

J. E. Shaheen (RW-44)
Outreach Programs
Office of Policy, Integration and
Outreach
U.S. Department of Energy
Forrestal Building
Washington, DC 20585

J. O. Neff, Manager
Salt Repository Project Office
U.S. Department of Energy
505 King Avenue
Columbus, OH 43201

D. C. Newton (RW-23)
Engineering & Licensing Division
Office of Geologic Repositories
U.S. Department of Energy
Forrestal Building
Washington, DC 20585

S. A. Mann, Manager
Crystalline Rock Project Office
U.S. Department of Energy
9800 South Cass Avenue
Argonne, IL 60439

O. L. Olson, Manager
Basalt Waste Isolation Project Office
U.S. Department of Energy
Richland Operations Office
Post Office Box 550
Richland, WA 99352

K. Street, Jr.
Lawrence Livermore National
Laboratory
Post Office Box 808
Mail Stop L-209
Livermore, CA 94550

D. L. Viath, Director (4)
Waste Management Project Office
U.S. Department of Energy
Post Office Box 14100
Las Vegas, NV 89114

L. D. Ramspott (3)
Technical Project Officer for NNWSI
Lawrence Livermore National
Laboratory
P.O. Box 808
Mail Stop L-204
Livermore, CA 94550

D. F. Miller, Director
Office of Public Affairs
U.S. Department of Energy
Post Office Box 14100
Las Vegas, NV 89114

W. J. Purcell (RW-20)
Office of Geologic Repositories
U.S. Department of Energy
Forrestal Building
Washington, DC 20585

D. A. Nowack (12)
Office of Public Affairs
U.S. Department of Energy
Post Office Box 14100
Las Vegas, NV 89114

D. T. Oakley (4)
Technical Project Officer for NNWSI
Los Alamos National Laboratory
P.O. Box 1663
Mail Stop F-619
Los Alamos, NM 87545

B. W. Church, Director
Health Physics Division
U.S. Department of Energy
Post Office Box 14100
Las Vegas, NV 89114

W. W. Dudley, Jr. (3)
Technical Project Officer for NNWSI
U.S. Geological Survey
Post Office Box 25046
418 Federal Center
Denver, CO 80225

Chief, Repository Projects Branch
Division of Waste Management
U.S. Nuclear Regulatory Commission
Washington, D.C. 20555

NTS Section Leader
Repository Project Branch
Division of Waste Management
U.S. Nuclear Regulatory Commission
Washington, D.C. 20555

Document Control Center
Division of Waste Management
U.S. Nuclear Regulatory Commission
Washington, D.C. 20555

V. M. Glanzman
U.S. Geological Survey
Post Office Box 25046
913 Federal Center
Denver, CO 80225

P. T. Prestholt
NRC Site Representative
1050 East Flamingo Road
Suite 319
Las Vegas, NV 89109

M. E. Spaeth
Technical Project Officer for NNWSI
Science Applications
International, Corporation
2769 South Highland Drive
Las Vegas, NV 89109

SAIC-T&MSS Library (2)
Science Applications
International, Corporation
2950 South Highland Drive
Las Vegas, NV 89109

W. S. Twenhofel, Consultant
Science Applications
International, Corp.
820 Estes Street
Lakewood, CO 80215

A. E. Gurrola
General Manager
Energy Support Division
Holmes & Narver, Inc.
Post Office Box 14340
Las Vegas, NV 89114

J. A. Cross, Manager
Las Vegas Branch
Fenix & Scisson, Inc.
Post Office Box 15408
Las Vegas, NV 89114

N. E. Carter
Battelle Columbus Laboratory
Office of Nuclear Waste Isolation
505 King Avenue
Columbus, OH 43201

John Fordham
Desert Research Institute
Water Resources Center
Post Office Box 60220
Reno, NV 89506

J. B. Wright
Technical Project Officer for NNWSI
Westinghouse Electric Corporation
Waste Technology Services Division
Nevada Operations
Post Office Box 708
Mail Stop 703
Mercury, NV 89023

ONWI Library
Battelle Columbus Laboratory
Office of Nuclear Waste Isolation
505 King Avenue
Columbus, OH 43201

W. M. Hewitt, Program Manager
Roy F. Weston, Inc.
2301 Research Blvd., 3rd Floor
Rockville, MD 20850

H. D. Cunningham
General Manager
Reynolds Electrical &
Engineering Co., Inc.
Post Office Box 14400
Mail Stop 555
Las Vegas, NV 89114

T. Hay, Executive Assistant
Office of the Governor
State of Nevada
Capitol Complex
Carson City, NV 89710

R. R. Loux, Jr., Director (3)
Nuclear Waste Project Office
State of Nevada
Capitol Complex
Carson City, NV 89710

C. H. Johnson, Technical
Program Manager
Nuclear Waste Project Office
State of Nevada
Capitol Complex
Carson City, NV 89710

Dr. Martin Mifflin
Desert Research Institute
Water Resources Center
Suite 1
2505 Chandler Avenue
Las Vegas, NV 89120

Department of Comprehensive
Planning
Clark County
225 Bridger Avenue, 7th Floor
Las Vegas, NV 89155

Lincoln County Commission
Lincoln County
Post Office Box 90
Pioche, NV 89043

Community Planning and
Development
City of North Las Vegas
Post Office Box 4086
North Las Vegas, NV 89030

City Manager
City of Henderson
Henderson, NV 89015

V. J. Cassella (RW-22)
Office of Geologic Repositories
U.S. Department of Energy
Forrestal Building
Washington, DC 20585

N. A. Norman
Project Manager
Bechtel National Inc.
P. O. Box 3965
San Francisco, CA 94119

Flo Butler
Los Alamos Technical Associates
1650 Trinity Drive
Los Alamos, New Mexico 87544

1510 J. W. Nunziato
1511 G. G. Weigand
1512 J. C. Cummings
1513 D. W. Larson
1520 D. J. McCloskey
1530 L. W. Davison
1540 W. C. Luth
6300 R. W. Lynch
6310 T. O. Hunter
6310 NNWSICF
6311 L. W. Scully
6311 L. Perrine (2)
6312 F. W. Bingham
6313 T. E. Blejwas

Planning Department
Nye County
Post Office Box 153
Tonopah, NV 89049

Economic Development
Department
City of Las Vegas
400 East Stewart Avenue
Las Vegas, NV 89101

Director of Community
Planning
City of Boulder City
Post Office Box 367
Boulder City, NV 89005

Commission of the
European Communities
200 Rue de la Loi
B-1049 Brussels
BELGIUM

Technical Information Center
Roy F. Weston, Inc.
2301 Research Boulevard,
Third Floor
Rockville, MD 20850

R. Harig
Parsons Brinkerhoff Quade &
Douglas, Inc.
1625 Van Ness Ave.
San Francisco, CA 94109-3678

Dr. Madan M. Singh, President
Engineers International, Inc.
98 East Naperville Road
Westmont, IL 60559-1595

6314 J. R. Tillerson
6315 S. Sinnock
6332 WMT Library (20)
6430 N. R. Ortiz
3141 C. M. Ostrander (5)
3151 W. L. Garner (3)
8024 M. A. Pound
DOE/TIC (28)
(3154-3, C. H. Dalin)

